Chemical Science

ROYAL SOCIETY OF CHEMISTRY

REVIEW

View Article Online
View Journal

Cite this: DOI: 10.1039/d6sc01385f

Recent advances in VAT photopolymerization additive manufacturing of battery electrodes: towards high-resolution 3D-printed batteries

Sima Lashkari,[a] Antonio Dominguez-Alfaro [c] and David Mecerreyes [ab]

Additive manufacturing of battery components is a relatively new field mostly dominated by extrusion-based 3D printing technologies. Alternatively, vat photopolymerization is starting to be noticed by the battery research field since it can enable 3D printing of electrodes with fast processing and high resolution. The high resolution allows for free-form-factor, which is not achievable with conventional techniques such as slurry casting. Nevertheless, several challenges must be addressed before vat photopolymerization can be considered a viable method for battery research and manufacturing. In this review, we address several of these challenges and highlight strategies to overcome them, providing new insights. In addition, we present a comprehensive review of the current state of the art in vat photopolymerization–based 3D printing of battery components using different technologies. Its potential for the future development of new 3D microstructured energy storage devices, such as micro-batteries, lithium-, sodium-, and zinc-ion batteries, will be finally discussed.

Received 16th February 2026
Accepted 17th April 2026

DOI: 10.1039/d6sc01385f

rsc.li/chemical-science

Introduction

Batteries and electrochemical energy storage devices traditionally manufactured in the form of macroscopic coin cells, cylindrical or prismatic cells, are part of our day-to-day life. Nevertheless, the rapid growth of bioelectronics,[1,2] medical implants,[3] and wearable electronics[4] demands more adaptable and innovative energy storage solutions. These demands have promoted the development of new energy technologies, including microbatteries[5] for the miniaturization of electronic devices; structurally conformable and flexible battery for free-form-factor electronics;[6] and the simultaneous enhancement of both energy and power densities in conventional batteries to support high-performance electric vehicles[7,8] and grid-scale energy storage.

Given the limitations of the current energy storage production line, which is dominated by slurry-casting methods, battery performance is approaching its practical limits. As an alternative, additive manufacturing has recently enabled the fabrication of complex geometries with high resolution. The most common additive manufacturing methods are inkjet printing (IJP), direct ink writing (DIW), selective laser sintering (SLS), aerosol jet printing (AJP), fused deposition modelling (FDM), and vat photopolymerization (VAT) methods, such as stereolithography (SLA), digital light processing (DLP) and two-photon lithography (2 PP).[9–11]

Additive manufacturing of battery components is a relatively new field mostly dominated by extrusion-based additive manufacturing.[12,13] In contrast, VAT-based additive manufacturing, although still primarily at the laboratory scale, offers the highest resolution among additive manufacturing methods, enabling finely detailed microstructures, excellent surface finishes, rapid curing, and minimal material waste. However, the adoption of photopolymerization in energy-storage applications has been limited by the strong light absorbance of most conductive additives and active materials. This optical attenuation slows photopolymerization kinetics and reduces cure depth, creating significant challenges for printing highly loaded, functional battery architectures. Despite these constraints, the trajectory of recent publications indicates growing interest in VAT for 3D battery fabrication, particularly for applications where its intrinsic advantages are most impactful, such as microbatteries, free-form-factor devices, and structural batteries—areas in which conventional manufacturing approaches face inherent limitations.

Positioning of this review and novelty compared to prior literature

Battery 3D printing has recently attracted significant attention within the energy-storage community, leading to a rapid rise in high-impact review articles on the topic. A careful examination of these reviews reveals that the existing literature generally falls

[a]POLYMAT, University of the Basque Country UPV/EHU, Avenida Tolosa 72, Donostia-San Sebastian, Spain. E-mail: david.mecerreyes@ehu.eus
[b]IKERBASQUE–Basque Foundation for Science, 48013 Bilbao, Spain
[c]Instituto de Microelectrónica de Sevilla, IMSE-CNM, (CSIC Universidad de Sevilla), Av. Américo Vespucio 28, 41092 Sevilla, Spain

into six major categories. (1) Several reviews focus on the architectural design of 3D-printed energy-storage systems, including seminal contributions by Horowitz *et al.*[14] as well as Scheideler *et al.*[15] (2) Other reviews concentrate on specific battery chemistries, such as the works by Huo *et al.*[16] on lithium-ion batteries and Gao *et al.*[17] on zinc ion battery. (3) A number of studies provide a broad overview of 3D-printing techniques for energy-storage applications.[8–11] (4) Some reviews adopt a materials-centric perspective, discussing how particular classes of materials can be adapted for 3D-printed energy devices.[18,19] (5) Additional reviews focus on individual additive-manufacturing methods, such as inkjet and extrusion-based printing[20] as well as DIW approaches[21,22] for energy storage applications. And finally, (6) few reviews target specific performance bottlenecks in energy-storage systems including high mass loading electrodes[23] tortuosity engineering,[24] as well as interfacial optimization.[25]

To date, only one review has specifically addressed VAT for battery components.[26] In contrast, the present work aims to provide a more comprehensive and critically integrated perspective on the challenges and prospects of adapting VAT for additive manufacturing of battery components. Rather than summarizing individual studies, we emphasize the fundamental constraints unique to VAT 3D printing processes such as light attenuation, cure depth limitation, sedimentation *etc.*, and discuss how these factors shape the feasibility of printing functional electrochemical architectures. Towards this goal, we first provide an overview of the different VAT techniques and their achievable resolution, followed by a discussion of resin chemistries commonly employed in VAT-printed battery components. Because battery 3D printing remains technically demanding, we then outline the design rules and recurring failure modes of manufacturing battery electrodes and the common practices in the literature to overcome them. We subsequently review recent advances in VAT-printed anodes, cathodes, current collectors/supports, and electrolytes, organizing the discussion by component type. Finally, we highlight the importance of electrode architecture and structural design, supported by statistics on reported 3D-printed geometries and a comparison between VAT and other additive-manufacturing techniques. We conclude with a perspective on the future potential of VAT 3D printing for battery manufacturing, while outlining the key bottlenecks that must be addressed for broader adoption.

A general overview of different VAT 3D printing methods

The first ever lithographic fabrication of a solid, known as SLA, was patented by Chuck Hull in 1984.[27] In SLA, photopolymerization occurs at the focal point of a UV laser, which scans across the resin surface to selectively cure each cross-sectional layer. This process, known as vector scanning, builds the object layer by layer until the entire structure is complete.[28] This method can be performed using either a top-down or a bottom-up approach (Fig. 1a). The top-down method usually generates better print fidelity; nevertheless, it suffers from oxygen inhibition (*i.e.*, oxygen-generated inhibition of radical polymerization) and requires a large volume of photopolymerizable resin.[29] On the other hand, the bottom-up fabrication requires less resin and reduces the effect of oxygen inhibition; however, it is generally more challenging since every built layer needs to be detached from the vat and reintroduced into the resin.[30]

Mask projection methods are also layer-by-layer techniques; however, instead of using a focused laser beam as in vector scanning, the entire cross section of the object is cured at once by generating a dynamic digital photomask that selectively passes light according to the layer pattern.[28] Mask projection methods include techniques such as DLP (Fig. 1c), mask projection micro-stereolithography (MP-μSL), or continuous liquid phase production (CLIP; Fig. 1d). While MP-μSL is similar to DLP, it is optimized for microscale printing. CLIP, on the other hand, uses an oxygen-permeable window at the bottom of the vat to exploit oxygen inhibition and create a non-curing liquid interface between the vat and the printed part. This layer prevents the cured resin from attaching to the vat, thus eliminating the need to detach the build part,[37] making this method about 100× faster than DLP.[38] While layer-by-layer methods are based on linear light matter interaction, where the curing happens at the first encounter of resin with light, nonlinear light matter interaction can be exploited in volumetric printing which gives rise to voxel (*i.e.*, volumetric pixel) level spatial control, such as in 2 PP using multiphoton absorption.[39] 2 PP can directly generate the 3D structure inside the resin, leading to submicron level resolution (∼100 nm), Fig. 1b. Early volumetric 3D printing used multiple intersecting light beams to project a 3D interference pattern onto the photoresist, so curing occurs at the overlapping region where the light intensity reaches the cure threshold.[40] Although conceptually important, this method was largely limited to periodic lattice structures. Volumetric printing was later advanced by Kelly *et al.*[35] through the development of tomographic volumetric additive manufacturing. In this method, a series of 2D light patterns-generated from the 3D model *via* an amplitude encoding mask, are projected from multiple angles onto a rotating cylindrical resin encoding the 3D objects. This technique, called computed axial lithography (CAL), enables the fabrication of aperiodic geometries, although the resolution in the original implementation was limited to approximately 300 μm, Fig. 1e.

The tomographic techniques were further advanced by the Moser group to achieve a resolution of 80 μm by employing a low étendue illumination system and an integrated feedback system to monitor polymerization kinetics in real time.[41] The same group further evolved the method by replacing the standard amplitude mask with more efficient holographic phase modulation, which improves the light efficiency, resulting in short printing time and smaller feature size (∼31 μm) while also extending applicability to opaque or scattering resins.[42]

In contrast to tomographic volumetric additive manufacturing, xolography is a volumetric printing technique based on nonlinear, dual-wavelength photochemistry rather than tomographic reconstruction. It uses two intersecting light sheets of different wavelengths to trigger localized

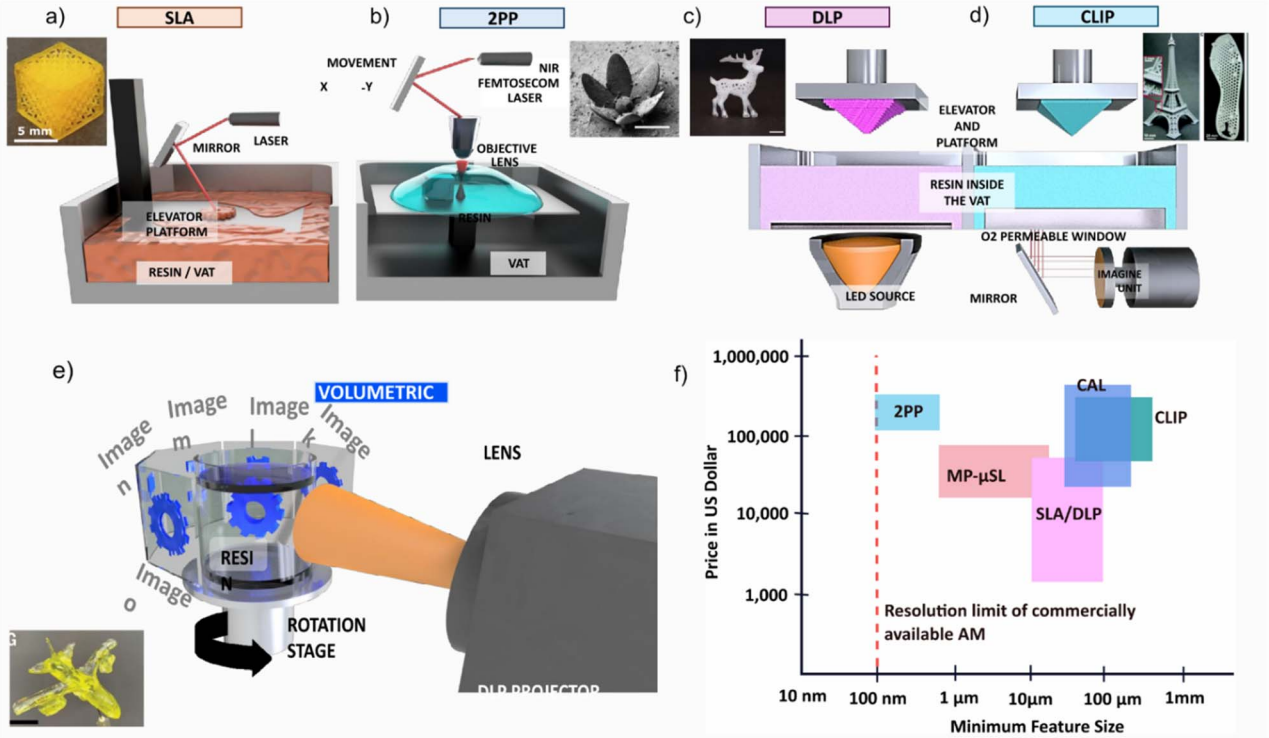

Fig. 1 Demonstration of VAT techniques and their basic differences, cost, resolution, mechanism, (a) SLA, inset shows a representative 3D object. Reproduced from ref. 31 with permission from American Chemical Society. Copyright© 2026 American Chemical Society. (b) 2PP, inset shows a representative 3D object, scale bar 40 µm. Reproduced from ref. 32 with permission from Springer Nature under a CC BY 4.0 licence. Copyright© 2022 Springer Nature. (c) DLP, inset shows a representative 3D object, scale bar 2 mm, Reproduced from ref. 33 with permission from Wiley-VCH under a CC BY 4.0 licence. Copyright© 2025 Wiley-VCH. (d) CLIP, inset shows a representative 3D object. Reproduced from ref. 34 with permission from AAAS. Copyright© 2012 AAAS. (e) CAL, inset show a representative 3D object, scale bar: 5 mm. Reproduced from ref. 35 with permission from AAAS. Copyright© 2019 AAAS. (f) Comparison between different VAT techniques in terms of cost and resolution. Concept based on ref. 36.

polymerization within a stationary vat of resin, enabling feature sizes as small as 20 µm.[43]

While the highest resolution is always desired, when choosing the right VAT method, the required resolution and cost must be considered. VAT is recognized for its superior spatial resolution and exceptional surface quality, attributes that are particularly advantageous in precision-demanding applications such as energy storage. As of now, SLA and DLP are the most widely used methods because they are more affordable and provide sufficient resolution (*i.e.*, ~10 µm). MP-µSL, a more precise and costly version of DLP, can reach a resolution of ~600 nm.[44] While CLIP improves the printing speed, commercial CLIP can only provide resolution in the range of 75–160 µm. Recently, single-digit-micrometre-resolution CLIP was developed, achieving a resolution of 1.5 µm.[45] However, CLIP is limited to low viscosity resins.[44] Volumetric techniques such as 2 PP and CAL can provide continuous AM in viscous resin, thus improving the printing speed as well as print fidelity and mechanical properties. In addition, unlike the layer-by-layer approach, volumetric VAT can create complex geometries without the need for support.[46] While CAL was originally developed for transparent resins, recent development has led to its application in ceramics as well as in light scattering resins.[44,47,48] This method can provide resolutions of 80 µm and 31 µm (for holographic techniques).[49] Fig. 1e compares different VAT techniques in terms of resolution and cost.

Photopolymerization chemistry in VAT 3D printing

The chemistry of the resins is crucial to address several issues related to VAT additive manufacturing. It typically relies on free-radical polymerization of a resin composed of multifunctional acrylic monomers or oligomers. Upon UV or visible-light exposure, the photoinitiator generates reactive radical species that initiate the polymerization of (meth)acrylate groups. This process rapidly forms a cross-linked polymer network, whose structure and mechanical properties depend on the monomer functionality and the radical kinetics. A typical resin formulation contains a mixture of mono-, di-, or trifunctional acrylate/methacrylate monomers, along with a photoinitiator chosen to match the light source of the specific 3D printer. Additional additives, such as reactive diluents or co-initiators, can be incorporated to tune polymerization kinetics and adjust the resin viscosity, thereby improving the resolution of printed structures. Among the wide family of acrylate-based inks, PEGDA is one of the most widely used due to its high reactivity, good solubility in aqueous and organic media, and its ability to produce homogeneous, mechanically tunable networks.[26]

As an alternative to free radical polymerization of acrylic monomers, thiol–ene polyaddition reactions[50,51] have gained significant attention in recent years in the field of VAT 3D printing. In this case, a cross-linked polymer network is formed *via* the step-growth addition of a multifunctional thiol to a multi-allyl (ene-functional) monomer. Other photopolymerization chemistries are also being actively explored for VAT 3D printing, including cationic polymerization of epoxides,[52] photobase- and photoacid-catalyzed ring-opening polymerizations of cyclic monomers such as thiolactones,[53] and photoinduced ring-opening metathesis polymerization (photo-ROMP) of cyclic olefins.[54,55] In addition, cyclopolymerization of difunctional cyclopolymerizable monomers[56] and cationic ring-opening polymerization of spiro-orthoesters[57] have been explored as low-shrinkage photopolymerization strategies. Furthermore, a recent comprehensive review by Thijssen *et al.*[58] explored synthetic routes toward photopolymerizable polyester-based systems, that can be applied in selected battery components.

Here, we attempt to briefly review the chemistries that are often used in battery manufacturing, to give the reader an overview of the attempted formulation; nevertheless, we stress that the future of battery 3D printing lies in developing new chemistries that more closely align with each battery technology (*e.g.* lithium ion, zinc or sodium batteries, *etc.*), and the required outcome.

Lithium-ion batteries have been the most extensively investigated energy-storage systems in battery 3D printing, predominantly using VAT-based techniques. These approaches commonly employ poly(ethylene glycol) diacrylate (PEGDA) as the primary monomer/crosslinker, in combination with photoinitiators such as lithium phenyl-2,4,6-trimethylbenzoylphosphinate (LAP) or 2,4,6-trimethylbenzoyldiphenylphosphine oxide (TPO). In some formulations, light absorbers such as tartrazine are added to mitigate excessive light penetration and over-curing, a known limitation of PEGDA-based resins.[59–61] Nevertheless, commercial acrylic resins such as Genesis have also been reported for printing both battery cathode and anode architectures.[62,63] Other acrylate chemistries, including urethane acrylate monomers (*e.g.*, Genomer 1122), urethane acrylate oligomers (*e.g.*, Allnex Abecryl 8210), and triacrylate monomers such as ethoxylated trimethylolpropane triacrylate (TMPTA), have been utilized when higher dimensional fidelity and controlled porosity are required.[64]

More recently, researchers working on Zn-ion batteries research has increasingly turned to 3D printing techniques, largely due to challenges associated with non-uniform Zn stripping/plating at the anode, which can lead to dendrite formation and internal short circuits. The use of periodic electrode architectures, such as gyroid structures, has been shown to mitigate these issues by homogenizing current density and suppressing localized Zn deposition. In addition, the increased electrode–electrolyte interfacial area provided by such periodic structures, when applied to both anodes and cathodes, can reduce ion concentration gradients and improve electrochemical stability. To date, preceramic polymers (*i.e.*, a photoresin composed of ceramic precursors and monomers) based on acrylate monomers have been explored for 3D printing of both anodes and cathodes, followed by post-processing or coating steps to incorporate electrochemically active materials.[65–67] In another study by Yu *et al.*, graphite oxide anodes were fabricated using a formulation consisting of acryloyl morpholine (monomer), 1,6-hexanediol diacrylate (HDDA, crosslinker), a polyurethane acrylate oligomer (PAO), and surfactant-modified graphene oxide as a filler, yielding improved dispersion and compositional homogeneity.[68]

Electrolyte development for VAT 3D printing has been explored for both lithium-ion and Zn-ion battery systems. For lithium-ion batteries, PEGDA-based formulations have been widely reported, often combined with photoinitiators such as LAP or TPO and liquid electrolytes.[69–72] Beyond its favourable printability, PEGDA is attractive due to the ability of its poly(ethylene oxide) segments to coordinate alkali metal ions, including Li^+ and Na^+, and facilitate salt dissociation, and enable ionic conductivity through segmental motion in the amorphous polymer domains.[73] Furthermore, the highly crosslinked nature of PEGDA networks can provide mechanical reinforcement that helps suppress lithium dendrite growth; this effect can be further tuned by incorporating additional multifunctional monomers such as TMPTA. Nevertheless, alternative chemistries have also been reported, including polyurethane acrylates[74] and systems based on *N*,*N*-dimethylacrylamide (DMAAm), a monofunctional acrylamide, crosslinked with divinylbenzene (DVB) and blended with poly(vinylidene fluoride) (PVDF).[75] To introduce controlled porosity, formulations combining PEO-μCTA with isobornyl methacrylate (IBoA) and acrylate monomers such as TMPTA have been explored.[76] Ceramic electrolytes have also been fabricated *via* 3D printing, often using commercial resins or HDDA-based formulations. For Zn-ion batteries, acrylamide and bis-acrylamide are commonly used as the monomer and crosslinker, respectively, forming polyacrylamide networks after polymerization. Polyacrylamide is highly hydrophilic, enabling efficient uptake of aqueous Zn electrolytes, while its compatibility with high-resolution VAT 3D printing allows the introduction of controlled porosity to further enhance electrolyte absorption.[77] In related formulations, acrylamide combined with *N*,*N*′-methylenebisacrylamide has been specifically employed to address non-uniform Zn deposition at the anode. The resulting polymer electrolytes provide tunable and precisely controlled axial pressure, which is critical for regulating Zn^{2+} nucleation kinetics and suppressing dendrite formation.[78] Fig. 2a summarizes the most common chemistries that are often used for VAT 3D printing of battery components.

In principle, all battery components can be fabricated using 3D printing. However, as illustrated in Fig. 2b, most reported studies have focused on printing electrodes and electrolytes. Compared with conventional slurry-casting methods, battery 3D printing offers significantly greater design freedom especially in solid-state battery design, such as tailoring of electrode/electrolyte interface to meet specific power requirements and the fabrication of shape-conformable or free-form-factor batteries (Fig. 2c and d). These aspects will be discussed in more detail in the following sections.

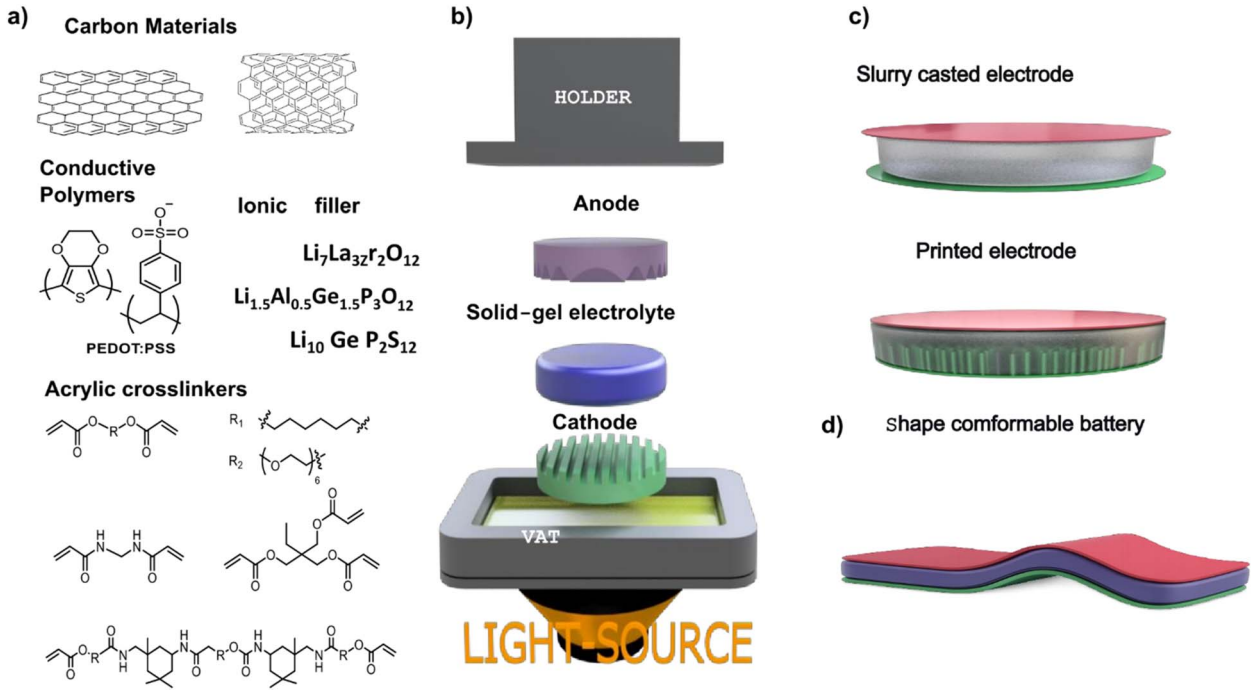

Fig. 2 3D printing of battery components chemistry and design, (a) common chemistries in VAT 3D printing of battery components, (b) 3D printing of common battery components enable precise control over battery architecture, (c) 3D printing of solid state batteries enables tailoring the porosities while slurry casted electrodes often lack interface engineering and high surface area required to achieve high power and energy densities, (d) flexible and shape conformable battery using battery 3D printing.

Design rules and common failure modes in VAT 3D printing of battery components

The primary advantage of 3D-printed batteries lies in the precise control over electrodes and electrolyte's three-dimensional architectures. Additive manufacturing enables the creation of well-defined geometries with increased surface area, uniform material distribution, tailored porosity, and periodic structural motifs. These features enhance ion transport, shorten diffusion pathways, and improve electrochemical homogeneity. As a result, 3D-printed batteries can significantly improve the utilization of active materials under high mass loading and mitigate issues such as volume expansion and dendrite formation in metal electrodes.

In solid-state batteries, 3D printing enables substantial enlargement of the electrode–electrolyte interfacial area, while providing flexible shape design and precise control over layer thickness (Fig. 2c and d), thereby improving ionic conductivity and interface stability.[79] Similarly, tailoring the effective surface area of the anode was shown to promote more uniform ion migration and reduce local current density.[80] Beyond lithium systems, additive manufacturing has been successfully applied to sodium and zinc batteries: in sodium-ion systems, 3D-printed Na metal electrodes accommodate volume fluctuations and foster uniform Na deposition, suppressing dendrite growth;[81] in aqueous zinc-ion batteries, 3D-printed architectures have helped overcome limitations related to low cathode loading and Zn dendrite formation.[82]

Despite these advances, most reported approaches rely on extrusion-based techniques, which inherently provide limited resolution and require inks with high viscosities and restricted formulation windows. High-resolution additive manufacturing—such as VAT 3D printing—can generate finely tuned geometries and hierarchical porosity at micro- and nanoscales, potentially enabling substantial increases in energy density.

It is worth noting that many of the challenges identified during the early development of VAT 3D printing, such as light scattering by suspended particles, sedimentation, increased viscosity, and limited cure depth, *etc.*, which limit the solid loading, remain highly relevant today. Addressing these issues requires solutions grounded in materials design, including careful control of chemical structure, optical properties, and rheological behaviour, as well as advances in processing and manufacturing strategies. Below, we summarize some of the most common challenges encountered in the VAT-based fabrication of battery components.

Solid electrolyte design

Ionic conductivity remains a critical bottleneck. Typically, solid gel electrolytes incorporate organic electrolytes, ionic liquids, or deep eutectic solvents, which must be embedded within polymeric matrices to achieve mechanically stable, three-dimensional architectures. This integration requires careful optimization to identify a formulation threshold that maintains sufficient ionic mobility without compromising the mechanical integrity or printability of the structure.

Anodes and cathodes

Both the anode and the cathode face several challenges during 3D printing, drying, and post-processing, such as pyrolysis.

Common issues that need to be addressed properly include curing gradient and efficiency, sedimentation of active battery materials, mechanical properties, shrinkage and changes in porosity, and cracks after pyrolysis due to an unoptimized debinding stage.

Curing gradient and efficiency: electrode design requires active materials as well as conductive materials such as carbon nanotubes, graphene, or PEDOT:PSS, among others, all of which are known for insolubility, poor dispersibility and strong optical absorption, which reduces penetration depth and curing efficiency of the polymers that compose the resin. Filler particles must negligibly contribute to light scattering and be adequately clear to allow satisfactory curing depth (C_d). Derived from the Beer–Lambert law, C_d can be expressed as eqn (1):

$$C_d = D_p \mathrm{Ln}(E_{max}/E_c) \quad (1)$$

where D_P is the penetration depth of light, E_{max} (J m^{-2}) is the exposure, and E_c (J m^{-2}) is the critical minimal exposure to initiate polymerization of the photocuring resin. In addition, as light passes through the resin medium, it is attenuated by scattering, adsorption, *etc.*, thereby reducing polymer conversion and causing a curing gradient. This physical phenomenon can be described using the Beer–Lambert law eqn (2):

$$I = I_0 e^{-\alpha x} \quad (2)$$

I is the transmitted light, I_0 is the incident light, α is the attenuation coefficient, and x is the light path length. This curing gradient often compromises the electrochemical performance of battery electrodes and must be addressed by properly optimizing the resin formulation and printing parameters. In addition, matching the photoinitiator to the resin can help improve curing issues. A comprehensive overview of photoinitiators is presented in a review by Bao, which also discusses overcoming the scattering issue in certain resins.[83]

Ink stability and sedimentation

As colloids, the resin formulations, particularly the anode and cathode, tend to sediment due to the large density difference between the active materials and the photosensitive resin, adversely affecting the homogeneity of the printed layers. Thus, it requires the proper selection of monomers and solvents to disperse the functional materials.

Mechanical properties

Tailored resin formulations are essential for electrode manufacturing to ensure stable mechanical performance. In electrode 3D printing, structural collapse can occur either during printing—due to insufficient or poorly controlled fluidity—or after drying, as a result of high solvent content in the formulation and shrinkage. Such a collapse can damage the electrode's porous architecture. Therefore, the resin must exhibit controlled fluidity (viscosity) during printing and sufficient mechanical robustness after drying to preserve structural integrity and pore morphology.

Pyrolysis and debinding steps

Pyrolysis is often used to remove extra polymer materials and make the electrode more conductive. Nevertheless, pyrolysis requires careful optimization, especially during the debinding stage, where polymeric materials are converted to carbonaceous materials to improve conductivity and active material loading. Cracks and shrinkage are very common in this step. While shrinkage can be compensated for by adjusting the printed electrode size, cracks, especially in the porous structure, are very common and sometimes difficult to avoid. Therefore, both the resin formulation and the calcination profile need to be optimized.

Different approaches in VAT 3D printing of battery electrode

Here, we outline the common strategies employed in VAT 3D printing to address these issues. Some of these approaches have already been applied in the battery field; however, many remain unexplored. In the following section, we first discuss these strategies in general terms and then examine their application to battery materials, with particular focus on electrochemical performance and their integration into components such as cathodes, anodes, and electrolyte.

Slurry method: directly mixing solid active materials with photo-curable resin

3D printing of ceramics and metals was initiated by directly mixing ceramic and metal nanoparticles with photo-curable resin[84] and it was later extended to energy storage applications.[85] To circumvent issues associated with the addition of suspended particles, active material loading was kept low, and thermal post-processing to sinter the nanoparticles and partially remove the polymer matrix was often followed by printing. Nevertheless, light scattering and the increased resin viscosity remain significant challenges, resulting in lower resolution compared to particle free resins. In addition, thermal treatment often results in anisotropic shrinkage and loss of original print dimensions caused by resin inhomogeneity.

Reducing the loading of active materials and conductive carbons often results in lower electronic conductivity, which can be addressed by modification of the filler, or chemically matching the filler and matrix. As electronic conductivity of the final electrode is of paramount importance for the functioning of the device, in the slurry based method, forming a percolating network can enhance the conductivity of the final 3D printed structure. As an illustrative example, Hensleigh *et al*[86]. developed a cross-linked graphene oxide (XGO) by ultrasonically dispersing a GO hydrogel monolith. A photoresin containing 1 wt% of this XGO mixed with acrylate monomer and photoinitiator can be 3D printed, forming final micro-architectured graphene after drying and pyrolysis. This method enables 3D printing complicated structures such as octet truss demonstrating superior conductivity of 60 S m^{-1} after pyrolysis. In addition, the unique 3D structure allows enhanced mechanical properties at reduced density.

Furthermore, the existing literature has disregarded the importance of the compatibility of the resin type with the filler

type, while, there are valuable studies show casing the importance of such compatibilities, which will enable reaching electrical percolation threshold before the rheological one. Using such strategy will ensure printability of the conductive resin. This was investigated by Sevriugina *et al.*[87] using aromatic and nonaromatic resin types combined with 0, 1 and 2D carbonaceous fillers (*i.e.* CB, MWNT, and graphene). The aromatic resin was demonstrated to induce stronger interaction between the MWNT and polymer resin, which leads to electrical percolation at lower filler concentration compared to rheological percolation–electrical percolation at 0.1 wt% filler *vs.* rheological percolation at 0.25 wt% filler.

Precursor approach: 3D printing of chemical precursors soluble in the 3D printed resins and generation of final electrode materials by thermal treatment

To address light-scattering issues associated with directly mixing active materials into photo-curable resins, a precursor approach has been introduced. In this method, chemical precursors of the active materials are either chemically embedded into the photocurable resin *via* various synthetic routes[67,88,89] or incorporated by mixing water-soluble precursor salts with the resin without chemical attachment (so-called chemical reactor method).[65] The resulting particle-free photoresist can be printed with high resolution owing to its homogeneity, low viscosity, and transparency. The 3D-printed parts then undergo thermal processing to form the final active materials, such as ceramics, metals, conductive additives, or inorganic battery compounds, with the advantage of isotropic shrinkage enabled by the homogeneous nature of the precursor resin.

Among the different methods, the chemical reactor method, pioneered by Yee *et al.*,[65] relied on the incorporation of precursor salt, often nitrate, into monomer matrix or cross-linkers such as polyethylene glycol diacrylate (PEGDA), together with the initiator. After 3D printing, the precursor remains unbound to the monomer, and the 3D-printed body acts as a "chemical reactor," allowing the synthesis of inorganic active materials during post-thermal processes. Using this approach, nanoparticle-free resins have been demonstrated to yield ZnO structures with feature sizes down to ~250 nm *via* 2 PP.

As an alternative to the previous case, chemical integration of the precursor into the monomer or polymer backbone has also been attempted. This concept was pioneered by the use of preceramic polymers in 3D printing,[88] which contain polymer chains with ceramic backbones (*e.g.*, polysilazanes, polycarbosilanes), serving as precursors for generating inorganics.[66] This principle was subsequently extended to metals, where ligand–exchange reactions between metal alkoxides and acrylic acid produced metal–acrylate resins suitable for high-resolution printing of nickel (25–100 nm features, ~90% purity).[67] Similarly, this route has been applied to TiO_2 (rutile) and can be generalized to other elements.[90] More recently, metal–organic frameworks (MOFs) have been explored as precursors, where neutralization of alkaline MOFs with acrylic acid yielded photoresins that enabled 2PP printing of ZnO and Co_3O_4 with resolutions down to ~170 nm.[89]

Emulsion based stereolithography

Even though VAT 3D printing techniques can create sub-micron feature size enabling enhancement of the surface area, this method still falls short of providing high porosity that is required for certain battery applications due to the limitation of the current 3D printers or the ink itself. One strategy is to use a colloidal system like water in oil (W/O) dispersion, where the photo-curable resin acts as the oil phase while precursors are dissolved in the water phase. After 3D printing of the structure, the as-printed object demonstrates porosities, which can be tuned by changing the volume of the dispersed phase (*i.e.* using high shear mixing or fine-tuning the surfactant kind and amount).[91] This method is referred to as emulsion stereolithography.

Liquid phase infusion or infiltration method

Hydrogel infusion additive manufacturing (HIAM) supports the fabrication of microscale metal or alloy structures using a single photoresin formulation.[92] In this method, instead of incorporating the precursor directly into the photo-curable resin, the precursors are infused into a 3D-printed hydrogel by immersing the part in a precursor salt solution for an extended period. The pre-soaked structures are then calcined to produce the desired material.

Implosion Fabrication (ImpFab), developed by Oran *et al.*,[93] is conceptually similar to HIAM but does not require a final heat-treatment step, since nanoparticles are directly anchored onto the 3D-patterned structure. In this approach, hydrophilic nanoparticle dispersions—such as semiconductor or metal nanoparticles—are infiltrated into a 3D-patterned acrylate hydrogel containing reactive groups that act as anchoring sites. The entire construct is subsequently shrunk using either a salt or an acid solution, followed by dehydration, producing nanoscale features with approximately 100 nm resolutions.

Electrodeposition and coating on 3D printed support

Another interesting strategy to avoid adding active materials directly to the photocurable resin is to 3D print a base or support, often using preceramic polymers, and then coat the surface using further surface modification and deposition techniques. This method has been demonstrated for the fabrication of both anode and cathode.[94–96] Fig. 3 illustrates these methods.

Additive manufacturing of current collector/support, anodes, cathodes and electrolytes

In this section, the most common additive manufacturing strategies applied to the different components of battery cells, such as the electrolyte and cathode, are discussed. Although VAT 3D printing of some of these components, such as the cathode or current collector, is more challenging and requires several steps and strategies to overcome particle scattering and sedimentation, other parts, such as the electrolyte and, in some cases, the anode, are more straightforward.

Additive manufacturing of electrode support/current collector

3D printing of electrode supports or current collectors, followed by further surface modification or electrodeposition, can be

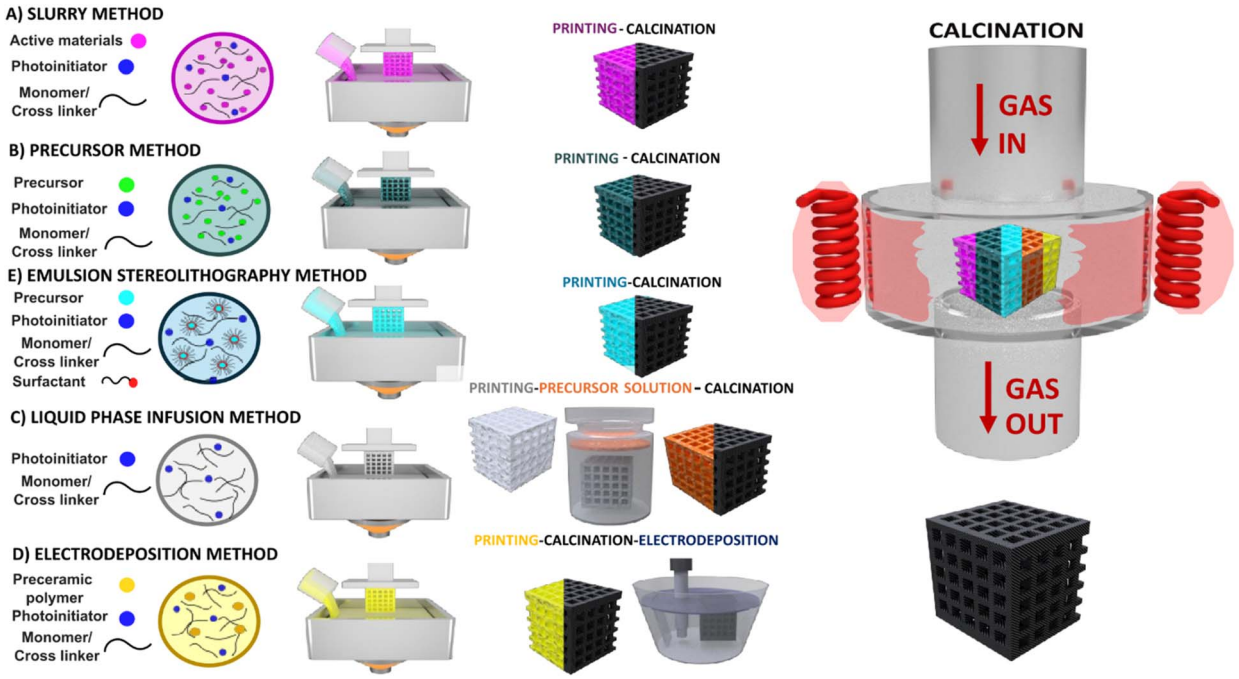

Fig. 3 Overview of different photopolymerization strategies used in VAT 3D printing of battery electrodes. For each method (left to right), the schematic illustrates the resin formulation, the VAT printing step, and the corresponding post-processing sequence. The right figure shows a tube furnace that is often applied for the calcination step in all the listed approaches (a) slurry method: the resin contains active materials dispersed in a photocurable matrix; post-processing typically involves calcination to remove organics and recover the functional phase. (b) Precursor method: the resin incorporates molecular or polymeric precursors of the active material together with the photocurable resin; post-processing includes calcination to convert the precursor into the electroactive phase. (c) Emulsion stereolithography: the resin formulation includes a photocurable phase, precursors of the active material, and surfactants to generate porosity; post-processing involves calcination to form the porous active structure. (d) Liquid-phase infusion method: the printed scaffold is produced from a photocurable resin without fillers; post-processing involves infiltration with an active-material precursor followed by calcination. (e) Electrodeposition-assisted method: the printed structure is typically based on preceramic polymers or photocurable resins; post-processing includes calcination and subsequent electrodeposition of the active material.

readily applied to fabricate both anode and cathode, often using a preceramic polymer resin. For instance, Zhang *et al.*[96] employed a preceramic polymer photoresin to improve the performance of the Zn ion battery by 3D printing a gyroid structure of silicon oxycarbide (SiOC) as a support for both the anode and the cathode. After printing the structure and pyrolysis, several surface modifications were applied, which render the surface conductive. Afterward, the negative and positive electrodes' active materials (*i.e.*, Zn and K_xMnO_2, respectively) were applied onto the support *via* either reduction of a precursor solution ($KMnO_4$) or electrodeposition of the active materials (Fig. 4a). This design minimizes the ion concentration gradient in the electrolyte, leading to more consistent striping plating of the zinc electrode and, eventually, improving the battery's performance in terms of both cycle life and capacity compared to using a Zn foil. Finally, with the optimized electrode design, the gyroid electrode structure can lead to improved performance, such as better capacity retention and coulombic efficiency.

A similar approach was taken by Wang *et al.*[95] in which a preceramic polymer resin support was printed using three types of periodic lattices (coincident, parallel, decussate). The as-printed lattice support was then calcinated to form SiOC and coated with Cu (SiOC@Cu). The final copper-plated support is then immersed in a Se-containing solution to generate the final electrode (SiOC@Cu_2Se). These electrodes showed high modulus and compressive strength, resulting in higher load-bearing capacity than the traditional two-dimensional electrode. This new design enables the use of a battery in conditions where constant mechanical pressure is applied.

Zhang *et al.*[94] have 3D printed alumina (alumina ceramic periodic surface substrates, abbreviated as ACPSS) with four different 3D structures (diamond, cubic, body-centered, and octet-truss periodic surface). The 3D-printed ACPSSs were copper-plated (Cu@ACPSS), followed by a second chemical bath to generate CuO/Cu@ACPSS electrodes. The final electrode was used as the cathode in a Zn-ion battery, with Zn foil as the anode. A volumetric capacity of 16.16 mA h cm^{-3} and coulombic efficiency of 95.49% after 60 cycles were achieved.

Martinez *et al.*[60] used a strategy similar to HIAM to 3D print a copper current collector by 3D printing the base resin, which consists of PEGDA/H_2O/TPO, dehydrating the green bodies, and soaking the dehydrated 3D structure in Cu precursor. After complete soaking of the precursors, the final structure was calcinated in air to remove the resin and reduced in H_2/Ar gas at 950 °C to generate pure copper. Electrophoretic deposition was

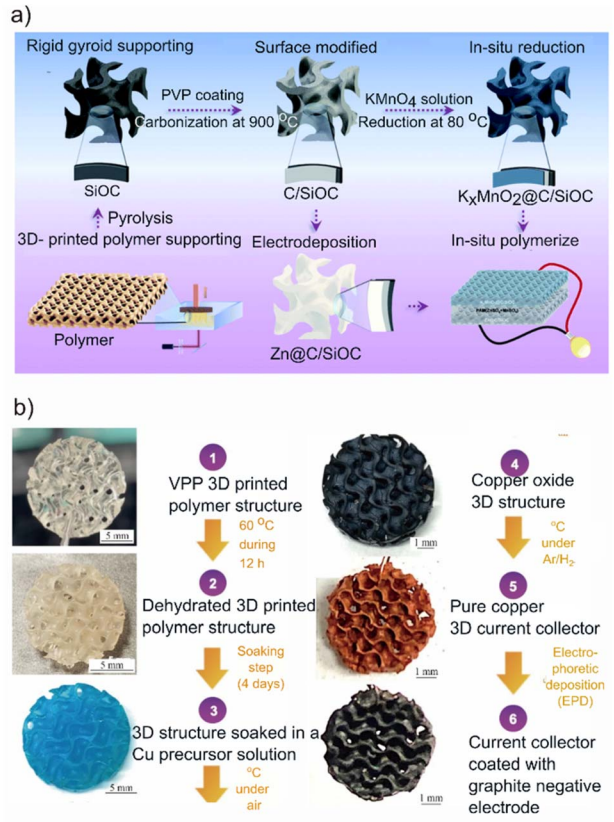

Fig. 4 Current collector/support additive manufacturing, (a) schematic illustration of the procedure for fabricating 3D gyroid electrodes and assembled solid-state ZIBs. Reproduced from ref. 96 with permission from the Royal Society of Chemistry. Copyright ©2022 Royal Society of Chemistry. (b) Optical images of the fabrication steps leading to a negative electrode coated onto a vat photopolymerization 3D printed current collector. Reproduced from ref. 63 with permission from Springer Nature under a CC BY licence. Copyright© 2024 Springer Nature.

then employed to deposit graphite onto the copper current collector (Fig. 4b). The anode was tested in a half-cell *vs.* lithium foil in liquid electrolyte. The first-cycle capacity of 371 mA h g^{-1} at *C*/20 is very close to the theoretical capacity of graphite (372 mA h g^{-1}), but with subsequent cycling, this capacity fades, and after the 60th cycle, around 100 mA h g^{-1} was retained (~73% capacity loss). This loss was associated with the gradual loss of active materials from the current collector.

Additive manufacturing of cathodes

Cathode fabrication in VAT-based AM has been attempted using several approaches such as precursor method, slurry method and emulsion stereo lithography.

Yee *et al.*[61] used the precursor approach (chemical reactor) to fabricate lithium cobalt oxide ($LiCoO_2$ or LCO) using lithium and cobalt nitrate aqueous photoresin in a DLP 3D printer to achieve precise geometry, which can be calcined to generate LCO with linear shrinkage of 40–50%. Using cubic lattice geometry with a 1 mm unit cell, around 100 mA h g^{-1} capacity was achieved, which retained 75% of its capacity after 130 cycles (Fig. 5a). Later on, Martinez *et al.*[59] used the same approach to 3D-print NMC 111. Similar to Yee's approach, they mixed nitrate salts of metallic elements in stoichiometric amounts in aqueous solution with a photoinitiator and a cross-linker (PEGDA).

After 3D printing the resin using DLP into an octahedral lattice structure, they used a thermal debinding method to synthesize NMC 111 and remove the inactive polymer binder and photoinitiator (Fig. 5b). The debinding step was critically studied, as it is fundamental to the electrode's final performance. Using an iterative approach, a capacity of around 100 mA h g^{-1} was reported at the *C*/10 rate.

Using emulsion stereolithography, Saccone and Greer[64] 3D printed a porous structure using an emulsion resin containing aqueous precursor $Li_2SO_4 \cdot H_2O$ as the water phase and photoresin as the oil phase. The 3D printed object undergoes post-pyrolysis to synthesize Li_2S (Fig. 5c). The final electrode features a 50 μm dimension and contains Li_2S active materials, whereas feature sizes smaller than 150 μm were not reported for AM of sulphur compounds. The final battery demonstrated a first-cycle discharge capacity of 310.1 mA h g^{-1}, 79.8% capacity retention after 100 cycles, and an average coulombic efficiency of 95.8%.

Martinez *et al.*[62] used the slurry method to 3D print an LCO cathode using the commercial resin (Genesis), Super C45 as conductive carbon and LCO as active materials. Three different inks were developed: a control ink without C45 (85 wt% resin, 15 wt% LCO), an experimental ink with good resolution (4.7 wt% LCO, 0.3 wt% C45, 95 wt% resin) and a primary ink with optimal electrochemical response (28 wt% LCO, 2 wt% C45, 70 wt% resin). The control ink highlighted the detrimental impact of C45 on the resin's printability, with concentrations as low as 1.5 wt% significantly impairing the printing process. The importance of the thermal post-processing is well demonstrated in this study, where the electrode demonstrated 62 mAh g^{-1} at *C*/50 in the green state, whereas after sintering, it was capable of delivering close to 160 mAh g^{-1} (Fig. 5b). However, the performance of the electrode in terms of the capacity retention still is not comparable to the commercial LCO electrode. As the dispersed particles were not stable in the ink, care was taken to reduce the maximum printing time in order to reduce the inhomogeneity of the final print, which pinpoints the challenges related to slurry-based method.

Using the precursor method, the AMs of both the cathode and the anode for aqueous Fe–Ni batteries were determined. Similar procedures were repeated for both the anode and the cathode, in which the iron or nickel substrate was first 3D printed using the precursor metal salt ($M_x(SO_4)_y$) in combination with the photocurable resin consisting of HDDA, E-TMPTA, and TPO. Then, the photoresin was 3D printed using DLP into a gyroid and lattice structure, and finally, the active materials were mounted on the substrate using a hydrothermal method in an autoclave, resulting in $NiCo_2S_4$@3DNi and Fe_3O_4@3DFe for the cathode and anode, respectively. Finally, the iron–nickel battery was assembled with aqueous electrolyte, achieving a high areal capacity of 7.32 mA h cm^{-2} at 44.85 mA cm^{-2} with 4 mm thick electrodes. The areal capacity was not affected by the electrode's thickness, which indicates the deconvolution of the electronic and ionic diffusion. In addition, the mechanical

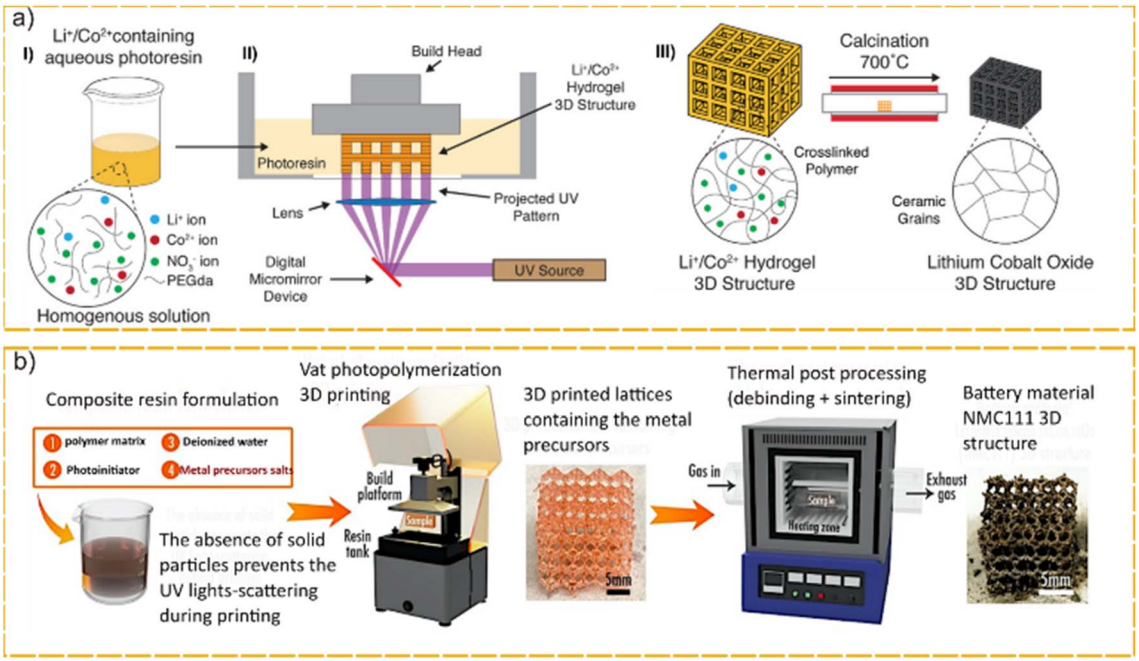

Fig. 5 Nanoparticle free photoresin for cathode fabrication, (a) (I) Schematic of DLP printing of a Li^+/Co^{2+} hydrogel 3D structure. (II) Schematic of DLP printing of a Li^+/Co^{2+} hydrogel 3D structure. (III) The 3D Li^+/Co^{2+} hydrogel is calcined to form a self-similar LCO structure. Reproduced from ref. 61 with permission from Wiley-VCH. Copyright© 2020 Wiley-VCH. (b) Main steps of the NMC 111 3D structures fabrication process. Reproduced from ref. 59 with permission from Springer Nature under CC BY 4.0 licence. Copyright© 2022 Springer Nature.

properties were vastly improved using smaller feature periodic structures.[97]

Additive manufacturing of anodes

Maurel *et al.*[63] used the slurry method for 3D printing of an anode containing TiO_2 for a lithium-ion battery. The resin consisted of a commercial methacrylate matrix (Genesis), Super C45, and 18 wt% TiO_2. A DLP 3D printer with the capability to restock the resin was found suitable, as the ink's viscosity hindered the printing process. Electrodes were printed in solid, cubic, and gyroid structures. The as-printed electrodes were sintered to increase conductivity to a reasonable value of 3.5 mS cm^{-1}, leading to specific capacities of 2 mA h g^{-1}, 122 mA h g^{-1}, and 164 mA h g^{-1} for solid, cubic, and gyroid structures, respectively (Fig. 6a). Both the cubic and the gyroid designs showed about a 60% capacity loss. The undesirable performance was attributed to the use of TiO_2 particles with an average diameter of 100 nm. This suggests that using smaller, nanosized particles with greater mesoporosity and potential for carbon coating could enhance performance.

VAT 3D printing can also be utilized in a less challenging approach to generate porous carbonaceous structures as anodes or electrodes for a double-layer capacitor. Narita *et al.*[98] have explored this strategy using a commercial acrylate-based resin. The printed electrode after pyrolysis was monolithic glassy carbon with strong mechanical properties, enabling the designed electrode to withstand the exerted pressure by the cell packaging (Fig. 6b). This method facilitates tailoring the electrode tortuosity and lithium ion diffusion length. Furthermore, by varying the number of unit cells in the electrode, the fraction of active material can be modified. The final electrode could reach the mass loading of 70 mg cm^{-2} and areal capacity of 3.2 mA h cm^{-2} at a current density of 2.4 mA cm^{-2}. By comparison with the graphite electrode, the 3D printed electrode shows lower overpotential and higher capacity.

In another study by Katsuyama *et al.*,[75] periodic micro-lattice structures were printed with an SLA 3D printer using a resin consisting of phenolic epoxy resin (41–53%), methacrylate monomer (21–42%), and photoinitiator (3–5%). The 3D-printed structure was further carbonized at 400 and 1000 °C for 4 h each (Fig. 6c). The resulting carbon micro-lattice anodes showed enhanced sodium-ion transport properties with 1 M NaPF6 electrolyte. The areal capacity that was achieved using this electrode was 21.3 mA h cm^{-2} at 98 mg cm^{-2} loading, which is much higher compared to the conventional monolithic electrode (5.2 mA h cm^{-2} at 92 mg cm^{-2}), Fig. 6d. For more information about the carbonization process applied to 3D-printed structures, the reader is referred to a comprehensive review by Onffroy *et al.*[99]

Yu *et al.*[100] reported the 3D printing of reduced graphite oxide using the slurry method as an anode material for aqueous zinc-ion batteries. The slurry was prepared using surfactant-functionalized graphite oxide in a photocurable resin containing acryloylmorpholine (ACMO), HDDA as a monomer and crosslinker, and PAO and TPO as photoinitiators. The resulting resin was 3D printed using the DLP method into a gyroid structure, and after heat treatment under N_2 in a furnace to remove polymers, it was electroplated with Zn in $ZnSO_4$ solution. The final anode (3DP-rGG@Zn) together with polyaniline-intercalated vanadium oxide (PVO) as the cathode was used for

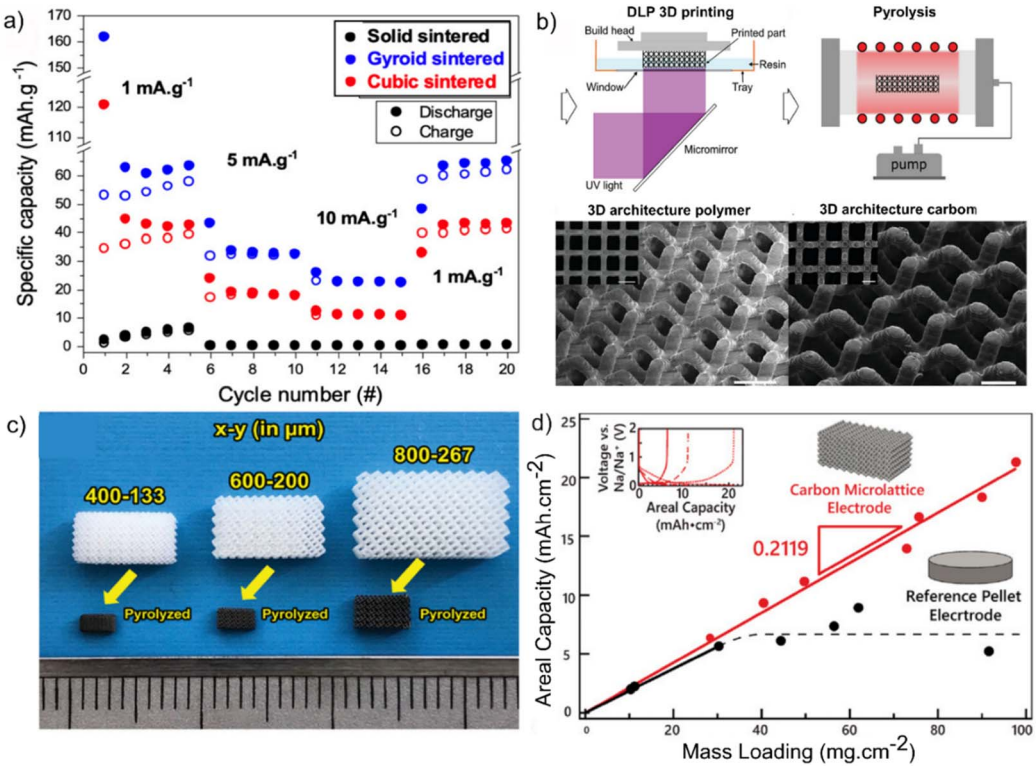

Fig. 6 Anode 3D printing, (a) TiO_2 anode for Li-ion battery, rate capability tests in half-cell configuration of the 3D printed electrodes fro sintered gyroid and cubic lattice as well as solid *vs.* sodium metal. Reproduced from ref. 63 with permission from the Electrochemical Society under a Creative Commons CC BY-NC 3.0 licence. Copyright© 2023 the Electrochemical Society. (b) Fabrication and images of 3D-architected carbon, as-fabricated 3D-architected polymer and its architected carbon replica. Reproduced from ref. 98 with permission from Wiley-VCH. Copyright© 2020 Wiley-VCH. (c) 3D-printed photo-cured resin (above) and its corresponding carbon micro-lattice electrodes (below). The minimum scale at the bottom is 1 mm. Reproduced from ref. 75 with permission from Wiley-VCH. Copyright© 2022 Wiley-VCH. (d) Areal capacity *vs.* mass loading for 3D printed carbon micro-lattice and reference pellet electrode. Reproduced from ref. 75 with permission from Wiley-VCH. Copyright© 2022 Wiley-VCH.

Zn–ion batteries. Using the 3D gyroid structure, the local current density distribution was controlled, resulting in uniform zinc deposition sites. This uniformity resulted in remarkably reversible striping plating over 1000 cycles at a high current density of 10 mA cm^{-2} for the half-cell anode. The full cell showed an outstanding capacity of 345.12 mA h cm^{-2}, which was retained for 1000 cycles (final capacity of 307.46 mA h cm^{-2}). In the following tale (Table 1), the summary of these methods and the chemistries used for the 3D printing of battery electrodes are listed.

As battery 3D printing is still in an early stage of development, there are wide discrepancies in the literature regarding key reported metrics such as density, porosity, loading, and capacity. While gravimetric capacity and architectural geometry are routinely documented, critical parameters such as active mass loading (mg cm^{-2}), electrode porosity, and bulk density are frequently omitted, hindering comparative analysis. It is important to emphasize that, in the context of battery 3D printing, these metrics are critical, as they dictate effective ion conductivities, tortuosity factors and achievable electrode mass loading. Furthermore, the lack of uniformity in testing conditions, specifically *C*-rates and current densities, often reflects individual laboratory protocols rather than standardized benchmarks. To facilitate a rigorous cross-study evaluation of emerging 3D-printing techniques, it is imperative to standardize these reporting parameters.

Additive manufacturing of solid electrolyte

VAT 3D printing of solid electrolyte is generally less challenging relative to that of the electrode, as the electrolyte does not need dark conductive additives or solid particles. The polymer electrolyte photoresin typically contains dissolved ions except ceramic-based hybrid solid electrolytes, which contain solid particles. To date, several strategies have been explored for 3D printing solid electrolyte: (1) blending the liquid electrolyte (such as IL, or conventional liquid electrolytes) with photo-curable resin, whether commercial or lab-formulated,[69–71,101–103] (2) chemically grafting the photo-polymerizable units onto an ionically conductive ionic liquids (IL),[104] or (3) incorporating lithium-conductive ceramic fillers into photo-curable matrices.[105–107] Employing photo-Reversible Addition–Fragmentation Chain Transfer (RAFT) polymerization induced micro-phase separation (PIMS), which enables control over both mechanical properties and ionic conductivities,[76,108] (4) soaking the 3D printed polymer structure into an electrolyte solution.[109]

Table 1 Summary of the reported methods of VAT-based additive manufacturing for battery electrodes[a]

Ref.	Active material-electrolyte	3D printing method	Function	Capacity	Electrode loading	Architecture	Resin type	Device/configuration	Resin materials	Density/porosity
96	K_xMnO_2@C/SiOCZn@C/SiOC	DLP	Support/cathode/anode	15.6 mA h cm^{-3} @ 5 mA cm^{-3}	NA	Gyroid	PDC	Zn ion battery, full cell	Acrylate based ceramic	NA
95	SiOC@Cu_2Se	DLP	Support/cathode	5.7 mA h cm^{-3} (1.046 mA h cm^{-2})[a] @ 4.88 mA cm^{-3}	NA	Periodic cubic lattice/parallel	PDC	Zn ion battery, half cell	Acrylate based ceramic	52–55.3% porosity
94	CuO/Cu@ACPSS	SLA	Support/cathode	31.95 mA h cm^{-3} (6.39 mA h cm^{-2})[a] @ 14 mA cm^{-3}	NA	Body centered periodic lattice	PDC	Zn ion battery, half cell	Acrylate based ceramic	66.8% porosity-1.34 g cm^{-3}
60	Cu@graphite	DLP	Current collector/anode	371 mA h g^{-1} @ 18.6 mA g^{-1}	NA	Gyroid	HIAM	Li ion battery, half cell	PEGDA/H_2O/TPO	NA
61	LCO	DLP	Cathode	121 mA h g^{-1} (6.05 mA h cm^{-2})[a] @ *C*6.85 mA g^{-1}	50 mg cm^{-2}	Cubic lattice	Precursor approach	Li ion battery, half cell	PEGDA/LAP/tartazine/precursor	56% porosity
59	NMC111	DLP	Cathode	98 mA h g^{-1} @ *C*/10	NA	Truncated octahedron cube	Precursor approach	Li-ion battery, half cell	PEGDA/TPO/precursor	NA
64	Li_2S–C	DLP	Cathode	310.1 mA h g^{-1} (0.403 mA h cm^{-2})[a] @ 58.25 mA g^{-1}	1.3 mg cm^{-2}	Octet microtruss lattice	Emulsion stereolithography	Li-sulfur battery, half cell	Genomer 1122/Mayzo OB+/Sartomer SR 494 LM/PL-TPO/Allnex Abecryl 8210/surfactant	84% porosity
62	$LiCoO_2$	DLP	Cathode	128 mA h g^{-1} @ 5.48 mA g^{-1}	NA	Gyroid	Slurry	Li-ion battery	Genesis/C45/LCO	NA
63	TiO_2	SLA	Anode	164 mA h g^{-1} (2.132 mA h cm^{-2})[a] @ 1 mA g^{-1} for gyroid	13–15 mg cm^{-2}	Gyroid/cubic	Slurry	Sodium ion battery, half cell	Genesis/TiO_2/C45	1.17 g cm^{-3} density
98	Carbon	DLP	Anode	3.2 mA h cm^{-2} @ 2.4 mA cm^{-2}	70 mg cm^{-2}	Octet lattice	Calcination	Li-ion battery	Acrylate based resin	0.1–0.35 g cm^{-3} density
75	Carbon	SLA	Anode	6.37 mA h cm^{-2} @ 5 mA g^{-1}	28 mg cm^{-2}	Carbon micro-lattice	Calcination	Sodium ion battery	Phenolic epoxy resin and methacrylate	NA
100	Graphite oxide@Zn	DLP	Anode	345.12 mA h cm^{-2} (5.39 mA h cm^{-2})[a] @ 5A g^{-1}	12.2 mg cm^{-2}	Gyroid	Slurry	Zn ion battery	ACMO/HDDA/PAO/, graphite oxide	NA
97	$NiCo_2S_4$@3DNi/Fe_2O_3@3DFe	DLP	Cathode and anode	7.32 mA h cm^{-2} at 44.85 mA cm^{-2}	18.38 mg cm^{-2}	Gyroid, lattice	Precursor approach	Ni–Fe battery	HDDA/E-TMPTA/metal precursor	0.8–1.7 g cm^{-3} density

[a] The values in parenthesis are calculated from the existing data.

3D printing of solid electrolyte was first reported by Schultz *et al.*[104] A phosphonium-based IL was co-polymerized with poly(ethylene glycol) dimethacrylate (PEGDMA) *via* photo polymerization using MP-μSL, which allowed the fabrication of complex structures with feature sizes ~400 μm. Using this method, several properties of the solid polymer electrolytes can be adjusted, such as glass transition temperature and ionic conductivity. Increasing the mol% of IL monomer and reducing that of PEGDMA (as in poly($PEGDMA_{60}$-*co*-$TOPTf_2N_{40}$) would increase the ionic conductivity to ~0.1 mS cm^{-1} at 150 °C and reduce the glass transition temperature (T_g) to −18 °C. While increasing PEGDMA (as in poly($PEGDMA_{90}$-*co*-$TOPTf2N_{10}$) resulted in reduced ionic conductivity (0.01 mS cm^{-1} at 150 °C), more cross-linked density, faster cure time and improved print fidelity (Fig. 7a).

Blending commercial liquid electrolytes with photoresins has emerged as the most straightforward and most frequently reported strategy for fabricating 3D-printed solid electrolytes. Simple mixing of sulfonated ILs with commercial methacrylate resins has yielded ionic conductivities up to 3.4 mS cm^{-1} at 90 °C.[102] Thiol-ene photopolymerization has also been employed, notably by Ahmed *et al.*,[101] achieving transparent, flexible, and thermally stable (220 °C) printed bodies with conductivities of 5.4 mS cm^{-1} at room temperature.

Alternative approaches include blending polymer matrices with salts and solvents. Rahman *et al.*[103] fabricated PVDF-based electrolyte with conductivities ranging from 0.35 to 0.65 mS cm^{-1} at room temperature which increased by one order of magnitude upon heating to 90 °C. 3D printed PEGDA–$NaClO_4$ composites for Na-ion batteries reached 0.3 mS cm^{-1} at room temperature.[71] Gel polymer electrolytes based on PEGDA mixed with liquid electrolytes (1 M $LiClO_4$ in EC/PC) have also been 3D printed, showing ~1 mS cm^{-1} conductivity at room temperature. The cathode and anode (*i.e.* LFP and LTO), were separately mixed with the electrolyte and were manually filled into the cathode and anode compartment of the solid electrolyte.[69] Structural optimization further improves performance. For example, He *et al.*[70] demonstrated that an archimedean lattice could be printed using PEGDA and liquid electrolyte composition. The resulting 3D-printed electrolyte exhibited an ionic conductivity of 0.3 mS cm^{-1} at room temperature. Half-cell tests comparing the Archimedean-structured electrolyte with a structure-less (bulk) counterpart revealed superior electrochemical performance in the former enabling higher cathode loadings. Maurel *et al.* tested the effect of MW of PEGDA in performance and printability. Using resin composition of PEGDA, TPO, succinonitrile (SCN) and $LiClO_4$ ionic conductivity and performance in lithium ion battery were tested. While higher MW improves the electrochemical performance, the print accuracy was adversely affected. The highest ionic conductivity of 9.2×10^{-2} mS cm^{-1} was achieved using a blend of 575 and 700 MW.[110] Blending of acrylamide monomer, *N*,*N*′ methylene bisacrylamid (MBA), LAP, tartazine (photo absorber dye) in 2 M $ZnSO_4$ solution and 3D printing using DLP, enabled

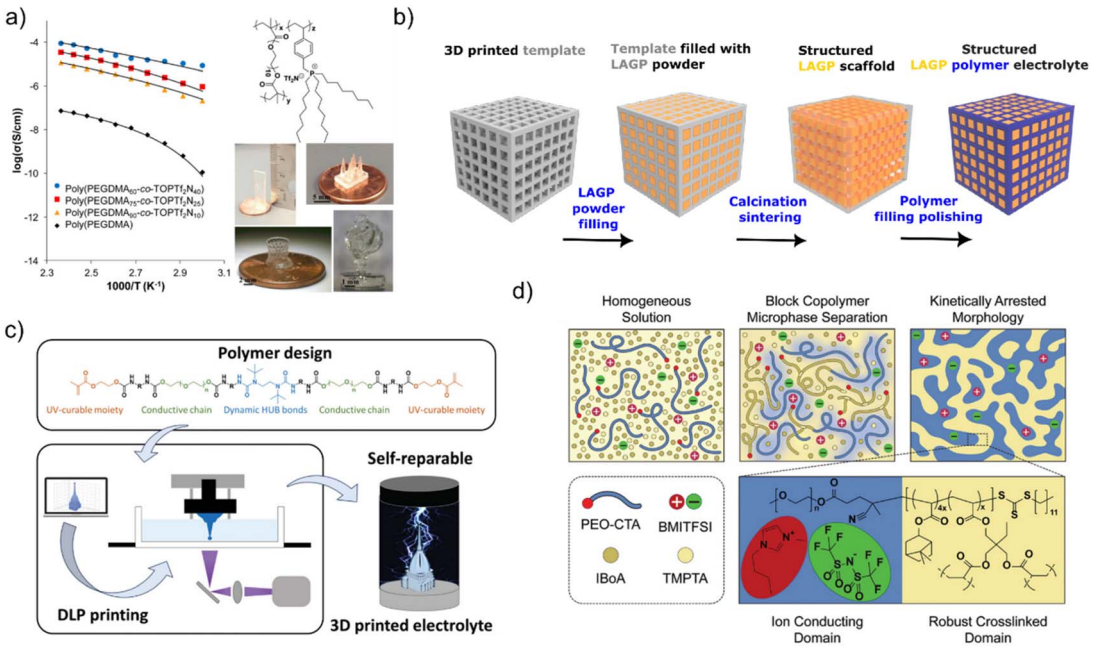

Fig. 7 Strategies for 3D printing of solid electrolyte, (a) co-polymerization of IL with PEGDMA, increasing the molar concentration of IL compared to that of PEGDMA increase the ionic conductivity of the solid electrolyte. Reproduced from ref. 104 with permission from American Chemical Society. Copyright© 2026 American Chemical Society. (b) Schematic of the templating procedure used for the synthesis of structured hybrid electrolytes with the example of the cube microarchitecture. Corresponding SEM images of each synthesis stage of cube LAGP–epoxy electrolytes are included below each schematic. Concept from ref. 105 (c) self-healable polymer electrolyte for 3D printing. Reproduced from ref. 109 with permission from Wiley-VCH under CC BY 3.0 license. Copyright©2024 Wiley-VCH (d) illustration of PIMS self-assembly process and resulting nanostructured material featuring ion-conducting channels (blue) and robust crosslinked domain (yellow). Reproduced from ref. 76 with permission from Wiley-VCH under CC BY-NC 4.0 licence. Copyright©2022 Wiley-VCH.

precise control over axial pressure on the anode side due to the capability of printing technique in generating precise thickness and surface finish in addition to fine porosity (3 micron). This pressure help improve interfacial properties of anode electrolyte interface (AEI) and improve cycle-ability of the cell even at high current density of 2 mA cm^{-2} over 1400 h.[78]

Beyond polymer-rich systems, hybrid and ceramic-based electrolytes have also been reported. Zekoll *et al.*[105] demonstrated performance of hybrid polymer/$Li_{1.5}Al_{0.5}Ge_{1.5}P_3O_{12}$ (LAGP) electrolyte using several 3D architectures of gyroid, cubic lattice, *etc.*, amongst which the gyroid structure showed the highest mechanical resilience and ionic conductivity of 0.16 mS cm^{-1} at room temperature (Fig. 7b). Karuppiah *et al.*[106] fabricated honeycomb-structured tantalum-doped $Li_7La_3Zr_2O_{12}$ (LLZO). They were able to print a honeycomb structure with minimum feature size of ~800 μm. This electrolyte reaches ionic conductivity of 3.7 mS cm^{-1} at 25 °C, while Sabato *et al.*[107] achieved 6.4 mS cm^{-1} with corrugated LAGP architectures that increased interfacial surface area.

Elizalde *et al.*[109] have developed a photo-curable polymer based on a hindered urea bond (HUB), bonded with PEO (known for its ion-conducting ability) and end-capped with photo-curable methacrylate groups. The final polymer was mixed with PEGDA (MW = 575 g mol^{-1}) and photoinitiator 2,2-dimethoxy-2-phenylacetophenone (DMPA) to generate a photocurable resin with fast curing properties (around 0.9 s for normal layers printing). The as-printed part was further post-cured and swelled in liquid electrolyte (1 M $LiPF_6$ in EC/DEC) to impart ionic conductivity. The membrane demonstrated self-healing properties when exposed to mechanical damage (Fig. 7c). The effect of porosity and soaking time has been tested for Zn-ion battery solid electrolyte using polyacrylamide, *N*,*N*-dimethylformamide (DMF) and $LiClO_4$. Increasing the porosity (*i.e.* 0%, 20% and 40%) improves the ionic conductivity, while the swelling time shows an optimum time of 60 min, above which the conductivity starts reducing. An impressive room temperature ionic conductivity of 28.10 mS cm^{-1} was achieved.[111]

Polymerization-Induced Microphase Separation (PIMS), originally developed by Seo and Hillmyer[112] and later applied to solid polymer electrolytes (SPEs),[113] enables the formation of nanostructured electrolytes with decoupled mechanical and transport properties, a feature desired in developing SPE for lithium metal batteries.[113] In this approach, as the block-*co*-polymer formation initiates, spontaneous micro-phase separation (thermodynamically driven) segregates the ion-conducting domain from the mechanically robust domain. The presence of cross-linker causes kinetic arrest of the self-assembled structure, forming two distinct micro-phase separated domains, an ion conducting domain (which contains PEO solvated IL) and a mechanically robust domain.

Recent advances using photo-RAFT PIMS (Boyer's group) highlight its potential for 3D-printed SPEs. Lee *et al.*[76] used photo-RAFT PIMS to generate SPE with both high module and high conductivity. In this study, PEO-μCTA was mixed with IBoA as the monomer, together with a cross-linker, a photoinitiator, and BMITFSI as the electrolyte. The choice of IBoA as a monomer is crucial for the final self-assembled structure. Having high T_g and hydrophobicity would ensure the rigidity of the final SPE. Moreover, its bulky structure would hinder tight molecular packing, resulting in a network with high void volume and the formation of micro-pores, which facilitate ion transport. As the kinetically arrested self-assembled structure is formed, IL would preferentially relocate to the PEO phase, creating a so-called PEO solvated IL (Fig. 7d). Using this method, the 3D printed gyroid lattice structure SPE demonstrates both high modulus and high ionic conductivity (*i.e.* 0.3 mS cm^{-1} and 1 mS cm^{-1} at RT and 90 °C, respectively). Structural tuning *via* branched *vs.* linear macro-CTAs (*e.g.*, PEO-μCTA *vs.* POEGMEA-μCTA) further allows balancing conductivity, modulus, and printability. While the ionic conductivities improved up to 1 order of magnitude using the branched μCTA (up to 1.2 mS cm^{-1} at 30 °C), the storage module was reduced compared to the linear PEO-μCTA. These studies underscore PIMS as a powerful strategy to engineer SPEs with nanoscale control, enabling simultaneous improvements in conductivity, mechanical robustness, and additive manufacturing compatibility.[108] Table 2 lists the studies related to VAT 3D printing of electrolyte.

Battery modelling and 3D architecture design

Currently, lithium-ion batteries have dominated the market due to their high energy density and long cycle life. However, their ionic diffusion (which determines power density) suffers significantly under the current manufacturing method (slurry casting), which produces two-dimensional electrodes. In the two-dimensional electrode, the energy and power densities are often interrelated, which limits the electrode loading to achieve full utilization of the active electrode material in the electrode's bulk. These limitations originate from slow interfacial kinetics and/or ohmic potential losses (related to small area-to-volume ratio and long ionic/electronic diffusion pathways, respectively).[114] To overcome this issue, often thin electrodes were adopted to increase the interfacial area, which severely affects the areal energy and power densities.[114]

The concept of electrode design, like an architect, was first introduced in the highly cited work by Long *et al.*[114,115] To think like an architect in electrode design requires the designer to consider both plumbing and wiring of the electrode (*i.e.* void space and electronic/ionic conductivity, respectively). By designing the electrode interior, a transition from 2D to 3D is possible, allowing access to charge-storing species throughout the electrode's volume and reducing the diffusional length of ions.

Another important aspect of electrode design is ensuring a uniform current–potential distribution throughout the electrode volume.[116] A uniform current potential distribution, specifically in the design of anode materials-can often lead to drastic improvement in the cycle life, coulombic efficiency and overall performance of the cell, as this non-uniformity often induces local dendrite growth and cell shortening.[117,118] The same issue in the design of the cathode can induce local current densities giving rise to underutilization and/or degradation of

Table 2 Summary of the reported methods of VAT-based additive manufacturing for battery solid electrolytes

Ref.	Materials	3D printing method	Function	Conductivity (mS cm^{-1})	Method
104	$TOPTf_2N$/BDA/PEGDMA/DMPA	MP-μSL	Electrolyte	0.01 at 60 °C	Polymerization of IL
76	PEO-μCTA/IBoA/TMPTA/TPO	DLP	Electrolyte	0.3 @ 22 °C	Photo-raft PIMS
108	POEGMEA-μCTA/IBoA/TMPTA/TPO	DLP	Electrolyte	1.2 @ 30 °C	Photo-raft PIMS
109	Poly(Urea-urathane)/PEGDA/DMPA	DLP	Electrolyte	3 @ 20 °C	Soaking in electrolyte
105	LAGP/commercial resin (IP–S)	SLA	Electrolyte	0.16 @ RT	Blending
106	LLZO/HDDA/Igracure 1173/Dispersant (BYK-2152)	DLP	Electrolyte	0.031 @ RT	Blending
107	LAGP/acrylate based commercial resin (Genesis)	SLA	Electrolyte	0.064 @ 25 °C	Blending
69	$LiClO_4$/EC/PC/PEGDA/BAPO	MP-μSL	Electrolyte	1 @ RT	Blending
101	IL/thiol–ene cross linker/acrylate monomer/Irgacure 127	SLA	Electrolyte	5.4 @ RT	Blending
102	Sulfonated-IL/commercial resin (FLGPCL02)	SLA	Electrolyte	0.07 @ RT	Blending
103	PVDF/DMAAm/EG/LiCl/DVB/kemisorp 11S/α-ketoglutaric acid	SLA	Electrolyte	0.65 @ RT	Blending
70	LiTFSI/SCN/PEGDA/BAPO	SLA	Electrolyte	0.3 @ RT	Blending
71	$NaClO_4$/EC/PC/PEGDA/TPO	SLA	Electrolyte	3.3 @ RT	Blending
111	Acrylamide/bis-acrylamide/LAP/$Zn(CF_3SO_3)_2/H_2O$	DLP	Electrolyte	28.10 @ RT	Soaking
74	Polyurethane acrylate resin/$LiClO_4$/DMF	SLA	Electrolyte	1.24 @ RT	Blending
110	PEGDA/SCN/$LiClO_4$/TPO	DLP	Electrolyte	0.092 @ RT	Blending
78	Acrylamide/MBA/LAP/tartazine/$ZnSO_4/H_2O$	DLP	Electrolyte	24.4 @ RT	Blending

active species.[119] Nevertheless, in 3D design, both geometrical length scale (such as electrode radius, length and spacing between electrodes) as well as materials properties (*e.g.* electronic conductivity) are required to be optimized.[114] The effect of the electric field of the electrode's double layer on the migration of ions through the electrolyte is also an important aspect that needs to be considered in design, which depends on the electrode's spacing and dimensions.[114] When architected properly, the 3D electrode can decouple the energy and power density; therefore, it would be possible to increase both without any compromise. Nevertheless, the 3D electrode design is still a new concept, which requires more in-depth analysis using computational modelling such as Finite Element Analysis (FEA). EFA uses numerical methods to analyse the effect of geometry on the current–potential distribution.[120,121] Other computational methods, such as the Vibrational Multiscale Method (VMS)[122] and Density Functional Theory (DFT),[123,124] focus on vibrational and atomic-level analyses, respectively. These techniques can link the local distribution of ions across the electrode to changes in local electrode properties.[115]

The literature frequently highlights methods such as porous templating,[125] inverse opal structures,[126] self-assembly,[127] and aerogel chemistry,[128] among others, for achieving a 3D electrode structure. However, these approaches are often labour-intensive, technically demanding, and difficult to scale. In addition, most of these methods are limited in their ability to create structural form factors (*i.e.*, restricted control over tortuosity) because they rely on physical laws or natural phenomena. In contrast, VAT-based 3D printing, particularly with recent advances in resolution, offers a more accessible and versatile alternative for fabricating complex architectures. This enables more in-depth investigation of ionic and electronic processes within electrodes, ultimately guiding the design of geometries that promote more uniform current and potential distributions. We refer readers to a study by Huddy *et al.*[129] in which different lattice structures were compared in terms of electronic conductivity, surface area, pore size, density, *etc.* Given the limitations of most 3D printing techniques, limited structural form factors can be achieved. These form factors often include simple structures such as grids, coils, disks, and interdigitated structures. However, given the high resolution and fine surface finish of recent VAT 3D printing methods such as 2 PP and MP-μSL, more complex geometries, such as gyroid and other cellular structures, can be designed, enabling further analysis of the effects of different geometries on the electrode's current–potential distribution. Fig. 8a and b compare the structural form factors achieved through VAT-based 3D printing with those produced by other 3D printing techniques, such as DIW, FDM, AIP, and IJP.

Summary and perspective

Here, a comprehensive review of the current state of the art in VAT–based 3D printing of battery components is presented. In recent years, additive manufacturing of battery components has been a highly evolving field, mostly dominated by extrusion-based 3D printing technologies. Alternatively, VAT 3D printing is increasingly being recognized for enabling fast, high-resolution electrode 3D printing. As highlighted in the last part of the review, recent advances in simulation and modeling are improving our understanding of electron and ion transport across diverse electrode architectures and battery form factors. These insights enable the emergence of novel designs with enhanced energy and power densities. In this context, high-resolution additive manufacturing techniques offer a promising pathway for realizing complex electrode architectures with precise, controllable form factors. Such architectures are not attainable using conventional slurry-casting methods, which are largely limited to non-reproducible, two-dimensional electrode films.

Nevertheless, several challenges need to be addressed before this method can be established as a standard method for

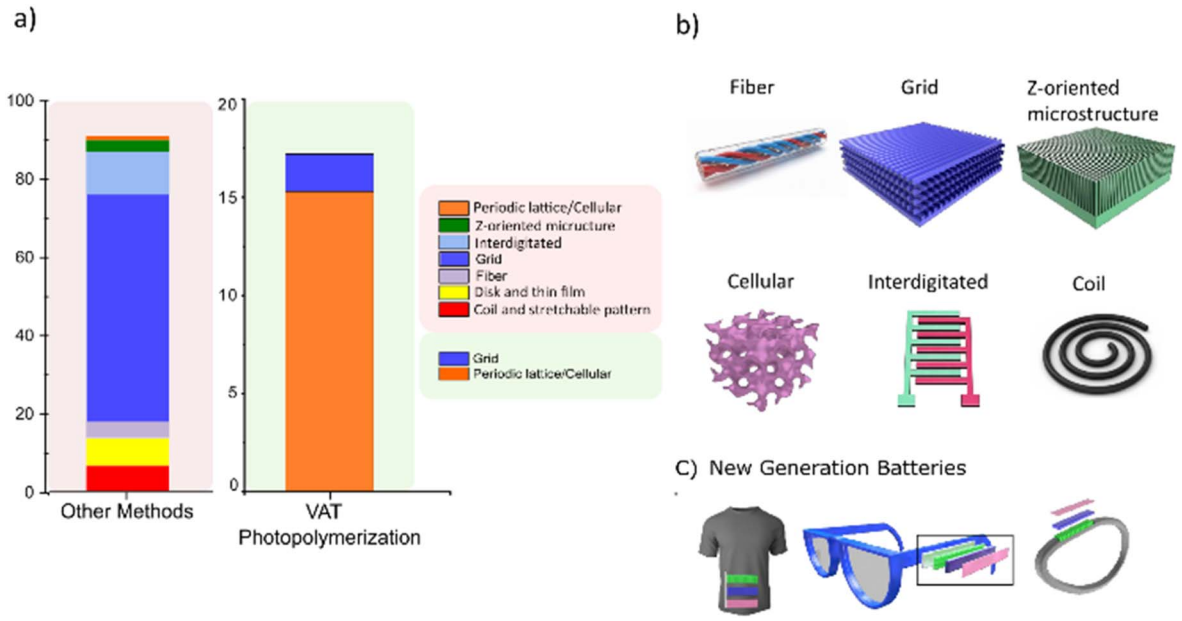

Fig. 8 Overview of structural design trends and emerging applications in 3D-printed battery architectures. (a) Stacked-column chart summarizing the reported 3D-printed electrode architectures fabricated using VAT photopolymerization and other additive-manufacturing methods. References for the studies included in this figure are provided in appendix I (SI). (b) Representative 3D electrode geometries enabled by different AM techniques. (c) Illustration of next-generation wearable and conformable electronics—such as garments, goggles, and wristbands—powered by integrated battery modules manufactured through additive-manufacturing approaches.

battery research and manufacturing. This is primarily because most energy storage active materials absorb and scatter light while also increasing the resin's viscosity, which hinders the printing process. In this review, we address several of these challenges and highlight the strategies developed to overcome them. To date, these limitations have been addressed by reducing the concentration of active materials in the slurry formulation or by using particle-free, precursor-based resins (so-called "chemical reactors"). Both approaches require post-processing, such as calcinations to remove excess polymer and synthesize the active materials. Alternative strategies, such as hydrogel infusion, additive manufacturing, and preceramic polymer resins, can be used for the additive manufacturing of the electrode, accompanied by further post-processing, such as active-material coating.

On the other hand, the recent progress of VAT 3D printing technologies has allowed to mitigate several limitations of the resins, such as high viscosity. For example, new SLA based additive manufacturing techniques, such as linear scan-based VAT 3D printing[130] enable 3D printing of high viscosity resins. Other emerging technologies,[131] such as multi-material printing, may offer solutions in the battery area. Multi-material 3D printing uses two different wavelengths of light simultaneously, enabling the fabrication of printed structures that cannot be achieved using conventional VAT 3D printing techniques such as DLP and SLA. Currently, the application of multi-material 3D printing has enabled additive manufacturing with two different materials from a single resin, for example 3D printing of soft *vs.* hard,[132] multicolor,[133] *etc.* Additionally, multi-material 3D printing can be used to improve the printing speed[134,135] and resolution by inhibiting over-curing, which is often a problem when printing with a single wavelength[136,137] Given the capabilities of multi-materials 3D printing, the future use of this new emerging technique can revolutionise battery manufacturing.

However, it is important to note that the broader adoption of these technologies as a manufacturing method will require careful consideration of several practical constraints, including low throughput, resin safety (particularly the handling of monomers and photoinitiators), reproducibility, quality control, and overall cost. Compared to conventional roll-to-roll or slurry-casting processes, the throughput of additive manufacturing remains limited due to the inherently slower layer-by-layer fabrication and the need for extensive post-processing. Materials safety also presents challenges, as many monomers and photoinitiators used in VAT 3D printing are toxic or irritant, complicating large-scale handling and storage. Furthermore, reproducibility is rarely reported in the literature even though VAT 3D printing is highly sensitive to small variations in resin formulation, light exposure, and processing conditions, factors that have not yet been demonstrated at an industrial scale. Finally, because the technology is still in an early stage of development, significant progress is needed before VAT 3D printing becomes economically viable for large-scale battery manufacturing.

All in all, additive manufacturing of battery components is a relatively new field mostly dominated by extrusion-based 3D printing technologies. The recent advances of VAT 3D printing technologies shown in this review anticipate that these technologies can play a role in the future development of 3D microstructured batteries.

Author contributions

Sima Lashkari led the conceptualization and development of the review, conducted the literature analysis, prepared the original manuscript draft, and carried out the major revisions in response to reviewer and co-author feedback. *Antonio Domínguez-Alfaro* contributed to figure preparation and provided critical revisions to the manuscript. *David Mecerreyes* supervised the project and contributed to manuscript review and editing.

Conflicts of interest

There are no conflicts to declare

Data availability

Supplementary information: Appendix I, which includes the references for Fig. 8a. See DOI: https://doi.org/10.1039/d6sc01385f.

Acknowledgements

This project has received funding from the European Union's Horizon 2020 research and innovation programme under the Marie Sklodowska – Curie grant agreement no. 10103429. AD-A acknowledges the Momentum grant, hired under the Generation D initiative, promoted by Red.es, an organisation attached to the Ministry for Digital Transformation and the Civil Service, for the attraction and retention of talent through grants and training contracts, financed by the Recovery, Transformation and Resilience Plan through the European Union's Next Generation funds. ID: MMT24-IMSE,CNM-02).

References

1 N. Fumeaux and D. Briand, 3D Printing of Customizable Transient Bioelectronics and Sensors, *Adv. Electron. Mater.*, 2024, **10**, 2400058.
2 S. Chen, W. S. Tan, M. A. Bin Juhari, Q. Shi, X. S. Cheng, W. L. Chan and J. Song, Freeform 3D printing of soft matters: recent advances in technology for biomedical engineering, *Adv. Electron. Mater.*, 2020, **10**, 453–479.
3 M. I. Alam, S. Kashyap, P. G. Balaji, A. K. Yadav and S. J. S. Flora, 3D-Printed Medical Implants: Recent Trends and Challenges, *Biomed. Mater. & Devices*, 2025, **3**, 750–770.
4 M. Jahandar, S. Kim and D. C. Lim, Transforming wearable technology with advanced ultra-flexible energy harvesting and storage solutions, *Nat. Commun.*, 2024, **15**, 8149.
5 J. Ma, S. Zheng, Y. Fu, X. Wang, J. Qin and Z.-S. Wu, The status and challenging perspectives of 3D-printed micro-batteries, *Chem. Sci.*, 2024, **15**, 5451–5481.
6 A. H. Espera, J. R. C. Dizon, Q. Chen and R. C. Advincula, 3D-printing and advanced manufacturing for electronics, *Progr. Addit. Manuf.*, 2019, **4**, 245–267.
7 C. Kim, B. Y. Ahn, S.-H. Cho, J.-W. Jung and I.-D. Kim, 3D Printing for Energy Storage Devices: Advances, Challenges, and Future Directions, *Adv. Mater.*, 2025, **37**, e05943.
8 C. Kim, B. Y. Ahn, S.-H. Cho, J.-W. Jung and I.-D. Kim, 3D Printing for Energy Storage Devices: Advances, Challenges, and Future Directions, *Adv. Mater.*, 2025, **37**, e05943.
9 V. Egorov, U. Gulzar, Y. Zhang, S. Breen and C. O'Dwyer, Evolution of 3D Printing Methods and Materials for Electrochemical Energy Storage, *Adv. Mater.*, 2020, **32**, 2000556.
10 N. Fonseca, S. V. Thummalapalli, S. Jambhulkar, D. Ravichandran, Y. Zhu, D. Patil, V. Thippanna, A. Ramanathan, W. Xu, S. Guo, H. Ko, M. Fagade, A. M. Kannan, Q. Nian, A. Asadi, G. Miquelard-Garnier, A. Dmochowska, M. K. Hassan, M. Al-Ejji, H. M. El-Dessouky, F. Stan and K. Song, 3D Printing-Enabled Design and Manufacturing Strategies for Batteries: A Review, *Small*, 2023, **19**, 2302718.
11 A. De, B. Ramasubramian, S. Ramakrishna and V. Chellappan, Advances in Additive Manufacturing Techniques for Electrochemical Energy Storage, *Adv. Mater. Technol.*, 2024, **9**, 2301439.
12 *The status and challenging perspectives of 3D-printed micro-batteries – Chemical Science*, RSC Publishing, https://pubs.rsc.org/en/content/articlelanding/2024/sc/d3sc06999k, accessed 29 January 2026.
13 *3D printing technology for rechargeable Li/Na-ion batteries – ScienceDirect*, https://www.sciencedirect.com/science/article/pii/S209549562400799X, accessed 29 January 2026.
14 Y. Horowitz, E. Strauss, E. Peled and D. Golodnitsky, How to Pack a Punch – Why 3D Batteries are Essential, *Isr. J. Chem.*, 2021, **61**, 38–50.
15 W. J. Scheideler and J. Im, Recent Advances in 3D Printed Electrodes – Bridging the Nano to Mesoscale, *Adv. Sci.*, 2025, **12**, 2411951.
16 S. Huo, L. Sheng, B. Su, W. Xue, L. Wang, H. Xu and X. He, 3D Printing Manufacturing of Lithium Batteries: Prospects and Challenges toward Practical Applications, *Adv. Mater.*, 2024, **36**, 2310396.
17 X. Gao, K. Liu, C. Su, W. Zhang, Y. Dai, I. P. Parkin, C. J. Carmalt and G. He, From bibliometric analysis: 3D printing design strategies and battery applications with a focus on zinc-ion batteries, *SmartMat*, 2024, **5**, e1197.
18 Y. Jiang, F. Guo, Y. Liu, Z. Xu and C. Gao, Three-dimensional printing of graphene-based materials for energy storage and conversion, *SusMat*, 2021, **1**, 304–323.
19 L.-H. Yu, X. Tao, S.-R. Feng, J.-T. Liu, L.-L. Zhang, G.-Z. Zhao and G. Zhu, Recent development of three-dimension printed graphene oxide and MXene-based energy storage devices, *Tungsten*, 2024, **6**, 196–211.
20 P. Yang and H. J. Fan, Inkjet and Extrusion Printing for Electrochemical Energy Storage: A Minireview, *Adv. Mater. Technol.*, 2020, **5**, 2000217.
21 T. Huang, W. Liu, C. Su, Y. Li and J. Sun, Direct ink writing of conductive materials for emerging energy storage systems, *Nano Res.*, 2022, **15**, 6091–6111.
22 Q. Zhang, J. Zhou, Z. Chen, C. Xu, W. Tang, G. Yang, C. Lai, Q. Xu, J. Yang and C. Peng, Direct Ink Writing of Moldable Electrochemical Energy Storage Devices: Ongoing Progress,

Challenges, and Prospects, *Adv. Eng. Mater.*, 2021, **23**, 2100068.
23 H. Yang, Z. Feng, X. Teng, L. Guan, H. Hu and M. Wu, Three-dimensional printing of high-mass loading electrodes for energy storage applications, *InfoMat*, 2021, **3**, 631–647.
24 X. Xue, D. Lin and Y. Li, Low Tortuosity 3D-Printed Structures Enhance Reaction Kinetics in Electrochemical Energy Storage and Electrocatalysis, *Small Struct.*, 2022, **3**, 2200159.
25 J. Bai, H. Li, P. Viveganantha, X. Tian, Y. Dong, J. Sun, Z. Dai and K. Zhou, Interface Engineering for 3D Printed Energy Storage Materials and Devices, *Adv. Energy Mater.*, 2024, **14**, 2303035.
26 *Toward High Resolution 3D Printing of Shape-Conformable Batteries via Vat Photopolymerization*, https://ieeexplore.ieee.org/document/9568946, accessed 22 March 2025.
27 C. W. Hull, *US Pat.*, US4575330A, 1986.
28 I. Gibson, D. W. Rosen and B. Stucker, *Additive Manufacturing Technologies: Rapid Prototyping to Direct Digital Manufacturing*, Springer US, Boston, MA, 2010.
29 R. Pynaert, J. Buguet, C. Croutxé-Barghorn, P. Moireau and X. Allonas, Effect of reactive oxygen species on the kinetics of free radical photopolymerization, *Polym. Chem.*, 2013, **4**, 2475–2479.
30 J.-C. Wang, M. Ruilova and Y.-H. Lin, in *2017 IEEE/SICE International Symposium on System Integration (SII)*, 2017, pp. 108–114.
31 L. Shahzadi, F. Maya, M. C. Breadmore and S. C. Thickett, Functional Materials for DLP-SLA 3D Printing Using Thiol–Acrylate Chemistry: Resin Design and Postprint Applications, *ACS Appl. Polym. Mater.*, 2022, **4**, 3896–3907.
32 K. Liu, H. Ding, S. Li, Y. Niu, Y. Zeng, J. Zhang, X. Du and Z. Gu, 3D printing colloidal crystal microstructures *via* sacrificial-scaffold-mediated two-photon lithography, *Nat. Commun.*, 2022, **13**, 4563.
33 J. Markhart, P. Mainik, P. S. Klee and E. Blasco, 4D Printing of Self-Immolative Polymers, *Adv. Funct. Mater.*, 2026, **36**, e20642.
34 J. R. Tumbleston, D. Shirvanyants, N. Ermoshkin, R. Janusziewicz, A. R. Johnson, D. Kelly, K. Chen, R. Pinschmidt, J. P. Rolland, A. Ermoshkin, E. T. Samulski and J. M. DeSimone, Continuous liquid interface production of 3D objects, *Science*, 2015, **347**, 1349–1352.
35 B. E. Kelly, I. Bhattacharya, H. Heidari, M. Shusteff, C. M. Spadaccini and H. K. Taylor, Volumetric additive manufacturing *via* tomographic reconstruction, *Science*, 2019, **363**, 1075–1079.
36 A. Zhakeyev, P. Wang, L. Zhang, W. Shu, H. Wang and J. Xuan, Additive Manufacturing: Unlocking the Evolution of Energy Materials, *Adv. Sci.*, 2017, **4**, 1700187.
37 R. Janusziewicz, J. R. Tumbleston, A. L. Quintanilla, S. J. Mecham and J. M. DeSimone, Layerless fabrication with continuous liquid interface production, *Proc. Natl. Acad. Sci. U. S. A.*, 2016, **113**, 11703–11708.
38 J. R. Tumbleston, D. Shirvanyants, N. Ermoshkin, R. Janusziewicz, A. R. Johnson, D. Kelly, K. Chen, R. Pinschmidt, J. P. Rolland, A. Ermoshkin, E. T. Samulski and J. M. DeSimone, Continuous liquid interface production of 3D objects, *Science*, 2015, **347**, 1349–1352.
39 Q. Thijssen, J. Toombs, C. C. Li, H. Taylor and S. Van Vlierberghe, From pixels to voxels: a mechanistic perspective on volumetric 3D-printing, *Prog. Polym. Sci.*, 2023, **147**, 101755.
40 M. Campbell, D. N. Sharp, M. T. Harrison, R. G. Denning and A. J. Turberfield, Fabrication of photonic crystals for the visible spectrum by holographic lithography, *Nature*, 2000, **404**, 53–56.
41 D. Loterie, P. Delrot and C. Moser, High-resolution tomographic volumetric additive manufacturing, *Nat. Commun.*, 2020, **11**, 852.
42 M. I. Álvarez-Castaño, A. G. Madsen, J. Madrid-Wolff, V. Sgarminato, A. Boniface, J. Glückstad and C. Moser, Holographic tomographic volumetric additive manufacturing, *Nat. Commun.*, 2025, **16**, 1551.
43 M. Regehly, Y. Garmshausen, M. Reuter, N. F. König, E. Israel, D. P. Kelly, C.-Y. Chou, K. Koch, B. Asfari and S. Hecht, Xolography for linear volumetric 3D printing, *Nature*, 2020, **588**, 620–624.
44 L. Stüwe, M. Geiger, F. Röllgen, T. Heinze, M. Reuter, M. Wessling, S. Hecht and J. Linkhorst, Continuous Volumetric 3D Printing: Xolography in Flow, *Adv. Mater.*, 2024, **36**, 2306716.
45 K. Hsiao, B. J. Lee, T. Samuelsen, G. Lipkowitz, J. M. Kronenfeld, D. Ilyn, A. Shih, M. T. Dulay, L. Tate, E. S. G. Shaqfeh and J. M. DeSimone, Single-digit-micrometer-resolution continuous liquid interface production, *Sci. Adv.*, 2022, **8**, eabq2846.
46 M. Shusteff, A. E. M. Browar, B. E. Kelly, J. Henriksson, T. H. Weisgraber, R. M. Panas, N. X. Fang and C. M. Spadaccini, One-step volumetric additive manufacturing of complex polymer structures, *Sci. Adv.*, 2017, **3**, eaao5496.
47 J. Madrid-Wolff, A. Boniface, D. Loterie, P. Delrot and C. Moser, Light-based Volumetric Additive Manufacturing in Scattering Resins, *Adv. Sci.*, 2022, **9**, 2105144.
48 M. Kollep, G. Konstantinou, J. Madrid-Wolff, A. Boniface, L. Hagelüken, P. V. W. Sasikumar, G. Blugan, P. Delrot, D. Loterie, J. Brugger and C. Moser, Tomographic Volumetric Additive Manufacturing of Silicon Oxycarbide Ceramics, *Adv. Eng. Mater.*, 2022, **24**, 2101345.
49 D. Loterie, P. Delrot and C. Moser, High-resolution tomographic volumetric additive manufacturing, *Nat. Commun.*, 2020, **11**, 852.
50 C. C. Cook, E. J. Fong, J. J. Schwartz, D. H. Porcincula, A. C. Kaczmarek, J. S. Oakdale, B. D. Moran, K. M. Champley, C. M. Rackson, A. Muralidharan, R. R. McLeod and M. Shusteff, Highly Tunable Thiol-Ene Photoresins for Volumetric Additive Manufacturing, *Adv. Mater.*, 2020, **32**, 2003376.

51 E. Rossegger, Y. Li, H. Frommwald and S. Schlögl, Vat photopolymerization 3D printing with light-responsive thiol-norbornene photopolymers, *Chem. Mon.*, 2023, **154**, 473–480.
52 M. Maturi, E. Locatelli, A. S. de Leon, M. C. Franchini and S. Ignacio Molina, Sustainable approaches in vat photopolymerization: advancements, limitations, and future opportunities, *Green Chem.*, 2025, **27**, 8710–8754.
53 O. Nuyken and S. D. Pask, Ring-Opening Polymerization—An Introductory Review, *Polymers*, 2013, **5**, 361–403.
54 S. C. Leguizamon, N. T. Monk, M. T. Hochrein, E. M. Zapien, A. Yoon, J. C. Foster and L. N. Appelhans, Photoinitiated Olefin Metathesis and Stereolithographic Printing of Polydicyclopentadiene, *Macromolecules*, 2022, **55**, 8273–8282.
55 J. C. Foster, A. W. Cook, N. T. Monk, B. H. Jones, L. N. Appelhans, E. M. Redline and S. C. Leguizamon, Continuous Additive Manufacturing using Olefin Metathesis, *Adv. Sci.*, 2022, **9**, 2200770.
56 L. A. Ruppitsch, G. Peer, K. Ehrmann, T. Koch and R. Liska, Photopolymerization of difunctional cyclopolymerizable monomers with low shrinkage behavior, *J. Polym. Sci.*, 2021, **59**, 519–531.
57 D. Kojic, K. Ehrmann, R. Wolff, Y. Mete, T. Koch, J. Stampfl, S. Baudis and R. Liska, Stereolithographic 3D printing of pure poly(ether–ester) networks from spirocyclic monomers *via* cationic ring-opening photopolymerization at high temperatures, *Polym. Chem.*, 2023, **14**, 4809–4818.
58 Q. Thijssen, A. Quaak, B. Bijleveld, B. Li, L. V. Daele, A. Heise and S. V. Vlierberghe, Light-Based 3D Printing of Polyesters: From Synthesis to Fabrication, *Chem. Rev.*, 2026, **126**, 1258–1293.
59 A. C. Martinez, A. Maurel, A. P. Aranzola, S. Grugeon, S. Panier, L. Dupont, J. A. Hernandez-Viezcas, B. Mummareddy, B. L. Armstrong, P. Cortes, S. T. Sreenivasan and E. MacDonald, Additive manufacturing of LiNi1/3Mn1/3Co1/3O2 battery electrode material *via* vat photopolymerization precursor approach, *Sci. Rep.*, 2022, **12**, 19010.
60 A. C. Martinez, A. Maurel, B. Yelamanchi, A. A. Talin, S. Grugeon, S. Panier, L. Dupont, A. Aranzola, E. Schiaffino, S. T. Sreenivasan, P. Cortes and E. MacDonald, Combining 3D printing of copper current collectors and electrophoretic deposition of electrode materials for structural lithium-ion batteries, *Adv. Manuf.*, 2025, **13**, 462–475.
61 D. W. Yee, M. A. Citrin, Z. W. Taylor, M. A. Saccone, V. L. Tovmasyan and J. R. Greer, Hydrogel-Based Additive Manufacturing of Lithium Cobalt Oxide, *Adv. Mater. Technol.*, 2021, **6**, 2000791.
62 A. C. Martinez, A. P. Aranzola, E. Schiaffino, E. MacDonald and A. Maurel, Additive manufacturing of $LiCoO_2$ electrodes *via* vat photopolymerization for lithium ion batteries, *Energy Adv.*, 2024, **3**, 1009–1018.
63 A. Maurel, A. C. Martinez, S. B. Chavari, B. Yelamanchi, M.-L. Seol, D. A. Dornbusch, W. H. Huddleston, S. T. Sreenivasan, C. G. Sherrard, E. MacDonald and P. Cortes, 3D Printed TiO_2 Negative Electrodes for Sodium-Ion and Lithium-Ion Batteries Using Vat Photopolymerization, *J. Electrochem. Soc.*, 2023, **170**, 100538.
64 M. A. Saccone and J. R. Greer, Understanding and mitigating mechanical degradation in lithium–sulfur batteries: additive manufacturing of Li_2S composites and nanomechanical particle compressions, *J. Mater. Res.*, 2021, **36**, 3656–3666.
65 D. W. Yee, M. L. Lifson, B. W. Edwards and J. R. Greer, Additive Manufacturing of 3D-Architected Multifunctional Metal Oxides, *Adv. Mater.*, 2019, **31**, 1901345.
66 B. J. Ackley, K. L. Martin, T. S. Key, C. M. Clarkson, J. J. Bowen, N. D. Posey, J. F. Ponder Jr, Z. D. Apostolov, M. K. Cinibulk, T. L. Pruyn and M. B. Dickerson, Advances in the Synthesis of Preceramic Polymers for the Formation of Silicon-Based and Ultrahigh-Temperature Non-Oxide Ceramics, *Chem. Rev.*, 2023, **123**, 4188–4236.
67 A. Vyatskikh, S. Delalande, A. Kudo, X. Zhang, C. M. Portela and J. R. Greer, Additive manufacturing of 3D nano-architected metals, *Nat. Commun.*, 2018, **9**, 593.
68 S. Yu, Y. Zhang, Y. Mu, B. Guo, G. Zeng, Y. Xiang, L. Zeng, J. Bai and J. Yang, Towards reusable 3D-printed graphite framework for zinc anode in aqueous zinc battery, *Energy Storage Mater*, 2024, **70**, 103454.
69 Q. Chen, R. Xu, Z. He, K. Zhao and L. Pan, Printing 3D Gel Polymer Electrolyte in Lithium-Ion Microbattery Using Stereolithography, *J. Electrochem. Soc.*, 2017, **164**, A1852.
70 Y. He, S. Chen, L. Nie, Z. Sun, X. Wu and W. Liu, Stereolithography Three-Dimensional Printing Solid Polymer Electrolytes for All-Solid-State Lithium Metal Batteries, *Nano Lett.*, 2020, **20**, 7136–7143.
71 A. C. Martinez, E. M. Schiaffino, A. P. Aranzola, C. A. Fernandez, M.-L. Seol, C. G. Sherrard, J. Jones, W. H. Huddleston, D. A. Dornbusch, S. T. Sreenivasan, P. Cortes, E. MacDonald and A. Maurel, Multiprocess 3D printing of sodium-ion batteries *via* vat photopolymerization and direct ink writing, *JPhys Energy*, 2023, **5**, 045010.
72 A. Maurel, C. A. Fernandez, E. M. Schiaffino, M. S. Mahmud, K. L. Delgado Ramos, Y. Lin, E. MacDonald, L. C. Merrill, J. A. Cardenas and A. C. Martinez, Vat photopolymerization three-dimensional printing of PEGDA/$LiClO_4$ solid polymer electrolytes with optimised accuracy and electrochemical-mechanical performance, *Virtual Phys. Prototyp.*, 2025, **20**, e2499480.
73 M. Armand, The history of polymer electrolytes, *Solid State Ionics*, 1994, **69**, 309–319.
74 M. F. Norjeli, N. Tamchek, Z. Osman, I. S. Mohd Noor, M. Z. Kufian and M. I. B. M. Ghazali, Additive Manufacturing Polyurethane Acrylate *via* Stereolithography for 3D Structure Polymer Electrolyte Application, *Gels*, 2022, **8**, 589.
75 Y. Katsuyama, A. Kudo, H. Kobayashi, J. Han, M. Chen, I. Honma and R. B. Kaner, A 3D-Printed, Freestanding

Carbon Lattice for Sodium Ion Batteries, *Small*, 2022, **18**, 2202277.

76 K. Lee, Y. Shang, V. A. Bobrin, R. Kuchel, D. Kundu, N. Corrigan and C. Boyer, 3D Printing Nanostructured Solid Polymer Electrolytes with High Modulus and Conductivity, *Adv. Mater.*, 2022, **34**, 2204816.

77 N. Poompiew, N. Jirawatanaporn, M. Okhawilai, J. Qin, A. J. Román, C. Aumnate, T. A. Osswald and P. Potiyaraj, 3D-printed polyacrylamide-based hydrogel polymer electrolytes for flexible zinc-ion battery, *Electrochim. Acta*, 2023, **466**, 143076.

78 Y. Zhou, W. Yuan, X. Wu, Q. Liu, X. Zhang, T. Gao, P. Wang, C. Li, G. Zhang, Y. Zeng and Y. Tang, Precise regulation of zinc-anode interface stresses by digital-light-processed gel polymer electrolytes for ultralong-life zinc batteries, *Int. J. Extrem. Manuf.*, 2025, **8**, 015507.

79 D. W. McOwen, S. Xu, Y. Gong, Y. Wen, G. L. Godbey, J. E. Gritton, T. R. Hamann, J. Dai, G. T. Hitz, L. Hu and E. D. Wachsman, 3D-Printing Electrolytes for Solid-State Batteries, *Adv. Mater.*, 2018, **30**, 1707132.

80 D. Cao, Y. Xing, K. Tantratian, X. Wang, Y. Ma, A. Mukhopadhyay, Z. Cheng, Q. Zhang, Y. Jiao, L. Chen and H. Zhu, 3D Printed High-Performance Lithium Metal Microbatteries Enabled by Nanocellulose, *Adv. Mater.*, 2019, **31**, 1807313.

81 Y. Yu, Z. Wang, Z. Hou, W. Ta, W. Wang, X. Zhao, Q. Li, Y. Zhao, Q. Zhang and Z. Quan, 3D Printing of Hierarchical Graphene Lattice for Advanced Na Metal Anodes, *ACS Appl. Energy Mater.*, 2019, **2**, 3869–3877.

82 H. Ma, X. Tian, T. Wang, K. Tang, Z. Liu, S. Hou, H. Jin and G. Cao, Tailoring Pore Structures of 3D Printed Cellular High-Loading Cathodes for Advanced Rechargeable Zinc-Ion Batteries, *Small*, 2021, **17**, 2100746.

83 Y. Bao, Recent Trends in Advanced Photoinitiators for Vat Photopolymerization 3D Printing, *Macromol. Rapid Commun.*, 2022, **43**, 2200202.

84 M. L. Griffith and J. W. Halloran, Freeform Fabrication of Ceramics *via* Stereolithography, *J. Am. Ceram. Soc.*, 1996, **79**, 2601–2608.

85 S. H. Park, M. Kaur, D. Yun and W. S. Kim, Hierarchically Designed Electron Paths in 3D Printed Energy Storage Devices, *Langmuir*, 2018, **34**, 10897–10904.

86 R. M. Hensleigh, H. Cui, J. S. Oakdale, J. C. Ye, P. G. Campbell, E. B. Duoss, C. M. Spadaccini, X. Zheng and M. A. Worsley, Additive manufacturing of complex micro-architected graphene aerogels, *Mater. Horiz.*, 2018, **5**, 1035–1041.

87 V. Sevriugina, D. Pavliňák, F. Ondreáš, O. Jašek, M. Štaffová and P. Lepcio, Matching Low Viscosity with Enhanced Conductivity in Vat Photopolymerization 3D Printing: Disparity in the Electric and Rheological Percolation Thresholds of Carbon-Based Nanofillers Is Controlled by the Matrix Type and Filler Dispersion, *ACS Omega*, 2023, **8**, 45566–45577.

88 J. Serbin, A. Ovsianikov and B. Chichkov, Fabrication of woodpile structures by two-photon polymerization and investigation of their optical properties, *Opt. Express*, 2004, **12**, 5221–5228.

89 J. Liu, Y. Liu, C. Deng, K. Yu, X. Fan, W. Zhang, Y. Tao, H. Hu, L. Deng and W. Xiong, 3D Printing Nano-Architected Semiconductors Based on Versatile and Customizable Metal-Bound Composite Photoresins, *Adv. Mater. Technol.*, 2022, **7**, 2101230.

90 A. Vyatskikh, R. C. Ng, B. Edwards, R. M. Briggs and J. R. Greer, Additive Manufacturing of High-Refractive-Index, Nanoarchitected Titanium Dioxide for 3D Dielectric Photonic Crystals, *Nano Lett.*, 2020, **20**, 3513–3520.

91 I. Cooperstein, M. Layani and S. Magdassi, 3D printing of porous structures by UV-curable O/W emulsion for fabrication of conductive objects, *J. Mater. Chem. C*, 2015, **3**, 2040–2044.

92 M. A. Saccone, R. A. Gallivan, K. Narita, D. W. Yee and J. R. Greer, Additive manufacturing of micro-architected metals *via* hydrogel infusion, *Nature*, 2022, **612**, 685–690.

93 D. Oran, S. G. Rodriques, R. Gao, S. Asano, M. A. Skylar-Scott, F. Chen, P. W. Tillberg, A. H. Marblestone and E. S. Boyden, 3D nanofabrication by volumetric deposition and controlled shrinkage of patterned scaffolds, *Science*, 2018, **362**, 1281–1285.

94 M. Zhang, T. Hu, P. Chang, Z. Jin, H. Mei, N. Dong and L. Cheng, 3D printing of CuO/Cu@Mullite electrodes with macroporous structures and their strong regulation on zinc ion storage, *Ceram. Int.*, 2022, **48**, 4124–4133.

95 X. Wang, M. Zhang, H. Mei, P. Chang and L. Cheng, Ultra-pressure-resistant SiOC@Cu2Se 3D printed cathode for aqueous zinc-ion batteries, *Ceram. Int.*, 2021, **47**, 24699–24706.

96 M. Zhang, T. Hu, X. Wang, P. Chang, Z. Jin, L. Pan, H. Mei, L. Cheng and L. Zhang, Boosting uniform charge distribution using 3D rigid electrodes with interconnected gyroid channels to achieve stable and reliable zinc-ion batteries, *J. Mater. Chem. A*, 2022, **10**, 7195–7206.

97 C. Li, J. Du, Y. Gao, F. Bu, Y. H. Tan, Y. Wang, G. Fu, C. Guan, X. Xu and W. Huang, Stereolithography of 3D Sustainable Metal Electrodes towards High-Performance Nickel Iron Battery, *Adv. Funct. Mater.*, 2022, **32**, 2205317.

98 K. Narita, M. A. Citrin, H. Yang, X. Xia and J. R. Greer, 3D Architected Carbon Electrodes for Energy Storage, *Adv. Energy Mater.*, 2021, **11**, 2002637.

99 P. R. Onffroy, S. Chiovoloni, H. L. Kuo, M. A. Saccone, J. Q. Lu and J. M. DeSimone, Opportunities at the Intersection of 3D Printed Polymers and Pyrolysis for the Microfabrication of Carbon-Based Energy Materials, *JACS Au*, 2024, **4**, 3706–3726.

100 S. Yu, Y. Zhang, Y. Mu, B. Guo, G. Zeng, Y. Xiang, L. Zeng, J. Bai and J. Yang, Towards reusable 3D-printed graphite framework for zinc anode in aqueous zinc battery, *Energy Storage Mater*, 2024, **70**, 103454.

101 K. Ahmed, N. Naga, M. Kawakami and H. Furukawa, Extremely Soft, Conductive, and Transparent Ionic Gels by 3D Optical Printing, *Macromol. Chem. Phys.*, 2018, **219**, 1800216.

102 K. Zehbe, A. Lange and A. Taubert, Stereolithography Provides Access to 3D Printed Ionogels with High Ionic Conductivity, *Energy Fuels*, 2019, **33**, 12885–12893.
103 M. S. Rahman, M. N. I. Shiblee, K. Ahmed, A. Khosla, J. Ogawa, M. Kawakami and H. Furukawa, Flexible and Conductive 3D Printable Polyvinylidene Fluoride and Poly(*N*,*N*-dimethylacrylamide) Based Gel Polymer Electrolytes, *Macromol. Mater. Eng.*, 2020, **305**, 2000262.
104 A. R. Schultz, P. M. Lambert, N. A. Chartrain, D. M. Ruohoniemi, Z. Zhang, C. Jangu, M. Zhang, C. B. Williams and T. E. Long, 3D Printing Phosphonium Ionic Liquid Networks with Mask Projection Microstereolithography, *ACS Macro Lett.*, 2014, **3**, 1205–1209.
105 S. Zekoll, C. Marriner-Edwards, A. K. O. Hekselman, J. Kasemchainan, C. Kuss, D. E. J. Armstrong, D. Cai, R. J. Wallace, F. H. Richter, J. H. J. Thijssen and P. G. Bruce, Hybrid electrolytes with 3D bicontinuous ordered ceramic and polymer microchannels for all-solid-state batteries, *Energy Environ. Sci.*, 2018, **11**, 185–201.
106 D. Karuppiah, D. Komissarenko, T. Thakur, N. Sena Yüzbasi, F. Clemens, E. Reisacher, P. Kaya, J. Pikul and G. Blugan, Vat photopolymerization of tantalum-doped $Li_7La_3Zr_2O_{12}$ electrolytes: a new Frontier in solid-state battery design, *J. Mater. Chem. A*, 2025, **13**, 387–398.
107 A. G. Sabato, M. N. Eroles, S. Anelli, C. D. Sierra, J. C. Gonzalez-Rosillo, M. Torrell, A. Pesce, G. Accardo, M. Casas-Cabanas, P. López-Aranguren, A. Morata and A. Tarancón, 3D printing of self-supported solid electrolytes made of glass-derived $Li_{1.5}Al_{0.5}Ge_{1.5}P_3O_{12}$ for all-solid-state lithium-metal batteries, *J. Mater. Chem. A*, 2023, **11**, 13677–13686.
108 D. Melodia, A. Bhadra, K. Lee, R. Kuchel, D. Kundu, N. Corrigan and C. Boyer, 3D Printed Solid Polymer Electrolytes with Bicontinuous Nanoscopic Domains for Ionic Liquid Conduction and Energy Storage, *Small*, 2023, **19**, 2206639.
109 F. Elizalde, S. Trano, J. Ayestarán, X. L. de Pariza, R. Aguirresarobe, C. Francia, D. Mecerreyes, H. Sardon, F. Bella and A. Light-Mediated, 3D-Printable, and Self-Healable Polymer Electrolyte for Lithium Batteries, *Adv. Funct. Mater.*, 2025, **35**, 2419034.
110 A. Maurel, C. A. Fernandez, E. M. Schiaffino, M. S. Mahmud, K. L. Delgado Ramos, Y. Lin, E. MacDonald, L. C. Merrill, J. A. Cardenas and A. C. Martinez, Vat photopolymerization three-dimensional printing of PEGDA/$LiClO_4$ solid polymer electrolytes with optimised accuracy and electrochemical-mechanical performance, *Virtual Phys. Prototyp.*, 2025, **20**, e2499480.
111 N. Poompiew, N. Jirawatanaporn, M. Okhawilai, J. Qin, A. J. Román, C. Aumnate, T. A. Osswald and P. Potiyaraj, 3D-printed polyacrylamide-based hydrogel polymer electrolytes for flexible zinc-ion battery, *Electrochim. Acta*, 2023, **466**, 143076.
112 M. Seo and M. A. Hillmyer, Reticulated Nanoporous Polymers by Controlled Polymerization-Induced Microphase Separation, *Science*, 2012, **336**, 1422–1425.
113 M. W. Schulze, L. D. McIntosh, M. A. Hillmyer and T. P. Lodge, High-Modulus, High-Conductivity Nanostructured Polymer Electrolyte Membranes *via* Polymerization-Induced Phase Separation, *Nano Lett.*, 2014, **14**, 122–126.
114 J. W. Long, B. Dunn, D. R. Rolison and S. W. Henry, *Three-Dimensional Battery Architectures*, https://pubs.acs.org/doi/full/10.1021/cr020740l, accessed 22 March 2025.
115 J. W. Long, B. Dunn, D. R. Rolison and H. S. White, 3D Architectures for Batteries and Electrodes, *Adv. Energy Mater.*, 2020, **10**, 2002457.
116 R. W. Hart, H. S. White, B. Dunn and D. R. Rolison, 3-D Microbatteries, *Electrochem. Commun.*, 2003, **5**, 120–123.
117 J. F. Parker, C. N. Chervin, E. S. Nelson, D. R. Rolison and J. W. Long, Wiring zinc in three dimensions re-writes battery performance—dendrite-free cycling, *Energy Environ. Sci.*, 2014, **7**, 1117–1124.
118 S. Li, M. Jiang, Y. Xie, H. Xu, J. Jia and J. Li, Developing High-Performance Lithium Metal Anode in Liquid Electrolytes: Challenges and Progress, *Adv. Mater.*, 2018, **30**, 1706375.
119 A. A. Talin, D. Ruzmetov, A. Kolmakov, K. McKelvey, N. Ware, F. El Gabaly, B. Dunn and H. S. White, Fabrication, Testing, and Simulation of All-Solid-State Three-Dimensional Li-Ion Batteries, *ACS Appl. Mater. Interfaces*, 2016, **8**, 32385–32391.
120 T. M. Clancy and J. F. Rohan, Simulations of 3D nanoscale architectures and electrolyte characteristics for Li-ion microbatteries, *J. Energy Storage*, 2019, **23**, 1–8.
121 D. Miranda, C. M. Costa, A. M. Almeida and S. Lanceros-Méndez, Computer simulations of the influence of geometry in the performance of conventional and unconventional lithium-ion batteries, *Appl. Energy*, 2016, **165**, 318–328.
122 S. Lee, A. M. Sastry and J. Park, Study on microstructures of electrodes in lithium-ion batteries using variational multi-scale enrichment, *J. Power Sources*, 2016, **315**, 96–110.
123 Y. Qi, L. G. Hector, C. James and K. J. Kim, Lithium concentration dependent elastic properties of battery electrode materials from first principles calculations, *J. Electrochem. Soc.*, 2014, **161**, F3010.
124 V. B. Shenoy, P. Johari and Y. Qi, Elastic softening of amorphous and crystalline Li–Si Phases with increasing Li concentration: a first-principles study, *J. Power Sources*, 2010, **195**, 6825–6830.
125 R. M. Penner and C. R. Martin, Controlling the Morphology of Electronically Conductive Polymers, *J. Electrochem. Soc.*, 1986, **133**, 2206.
126 J. S. Sakamoto and B. Dunn, Hierarchical battery electrodes based on inverted opal structures, *J. Mater. Chem.*, 2002, **12**, 2859–2861.
127 F. Cheng, Z. Tao, J. Liang and J. Chen, Template-Directed Materials for Rechargeable Lithium-Ion Batteries, *Chem. Mater.*, 2008, **20**, 667–681.

128 D. R. Rolison and B. Dunn, Electrically conductive oxide aerogels: new materials in electrochemistry, *J. Mater. Chem.*, 2001, **11**, 963–980.
129 J. E. Huddy, A. P. Tiwari, H. Zhao, Y. Li and W. J. Scheideler, Graph Theory Design of 3D Printed Conductive Lattice Electrodes, *Adv. Mater. Technol.*, 2023, **8**, 2300180.
130 Z. Weng, X. Huang, S. Peng, L. Zheng and L. Wu, 3D printing of ultra-high viscosity resin by a linear scan-based vat photopolymerization system, *Nat. Commun.*, 2023, **14**, 4303.
131 J.-W. Choi, H.-C. Kim and R. Wicker, Multi-material stereolithography, *J. Mater. Process. Technol.*, 2011, **211**, 318–328.
132 J. J. Schwartz and A. J. Boydston, Multimaterial actinic spatial control 3D and 4D printing, *Nat. Commun.*, 2019, **10**, 791.
133 K. C. H. Chin, G. Ovsepyan and A. J. Boydston, Multi-color dual wavelength vat photopolymerization 3D printing *via* spatially controlled acidity, *Nat. Commun.*, 2024, **15**, 3867.
134 M. Regehly, Y. Garmshausen, M. Reuter, N. F. König, E. Israel, D. P. Kelly, C.-Y. Chou, K. Koch, B. Asfari and S. Hecht, Xolography for linear volumetric 3D printing, *Nature*, 2020, **588**, 620–624.
135 V. Hahn, P. Rietz, F. Hermann, P. Müller, C. Barner-Kowollik, T. Schlöder, W. Wenzel, E. Blasco and M. Wegener, Light-sheet 3D microprinting *via* two-colour two-step absorption, *Nat. Photonics*, 2022, **16**, 784–791.
136 T. F. Scott, B. A. Kowalski, A. C. Sullivan, C. N. Bowman and R. R. McLeod, Two-Color Single-Photon Photoinitiation and Photoinhibition for Subdiffraction Photolithography, *Science*, 2009, **324**, 913–917.
137 Rapid, continuous additive manufacturing by volumetric polymerization inhibition patterning | Science Advances, https://www.science.org/doi/10.1126/sciadv.aau8723, accessed 1 December 2025.